ASL-TR-0074

AD

Reports Control Symbol
OSD 1366

AD A100386

DTIC FILE COPY

CHARACTERIZATION OF AEROSOL NONLINEAR EFFECTS ON A HIGH POWER CO_2 LASER BEAM

FEBRUARY 1981

By

C. W. BRUCE

Y. P. YEE

S. J. DURAN

DTIC

Approved for public release; distribution unlimited

US Army Electronics Research and Development Command
ATMOSPHERIC SCIENCES LABORATORY
White Sands Missile Range, NM 88002

81 6 30 020

NOTICES

Disclaimers

The findings in this report are not to be construed as an official Department of the Army position, unless so designated by other authorized documents.

The citation of trade names and names of manufacturers in this report is not to be construed as official Government indorsement or approval of commercial products or services referenced herein.

Disposition

Destroy this report when it is no longer needed. Do not return it to the originator.

(14) SECURITY CLASSIFICATION OF THIS PAGE (When Data Entered)

ERADCOM/ REPORT DOCUMENTATION PAGE

READ INSTRUCTIONS BEFORE COMPLETING FORM

1. REPORT NUMBER: ASL-TR-0074

2. GOVT ACCESSION NO.: AD A100886

3. RECIPIENT'S CATALOG NUMBER: (7)

4. TITLE (and Subtitle): (6) CHARACTERIZATION OF AEROSOL NONLINEAR EFFECTS ON A HIGH POWER CO_2 LASER BEAM,

5. TYPE OF REPORT & PERIOD COVERED: Final Report

6. PERFORMING ORG. REPORT NUMBER:

7. AUTHOR(s): (10) C. W. Bruce, S. J. Duran*, Y. P. Yee

8. CONTRACT OR GRANT NUMBER(s): (17) D 1

9. PERFORMING ORGANIZATION NAME AND ADDRESS: US Army Atmospheric Sciences Laboratory, White Sands Missile Range, NM 88002

10. PROGRAM ELEMENT, PROJECT, TASK AREA & WORK UNIT NUMBERS: (16) DA Task No. 1L161102D53AD1

11. CONTROLLING OFFICE NAME AND ADDRESS: (11) US Army Electronics Research and Development Command, Adelphi, MD 20783

12. REPORT DATE: Feb[redacted]81

13. NUMBER OF PAGES: 74

14. MONITORING AGENCY NAME & ADDRESS (if different from Controlling Office): (12) 72

15. SECURITY CLASS. (of this report): UNCLASSIFIED

15a. DECLASSIFICATION/DOWNGRADING SCHEDULE:

16. DISTRIBUTION STATEMENT (of this Report):

Approved for public release; distribution unlimited.

17. DISTRIBUTION STATEMENT (of the abstract entered in Block 20, if different from Report):

18. SUPPLEMENTARY NOTES:

*Physical Science Laboratory
New Mexico State University
Las Cruces, NM 88003

19. KEY WORDS (Continue on reverse side if necessary and identify by block number):

High power lasers
Aerosol absorption
Optoacoustic spectroscopy
Nonlinear effects
Countermeasure smoke

20. ABSTRACT (Continue on reverse side if necessary and identify by block number):

This report describes a set of aerosol measurements to determine the effect of a countermeasure smoke, white phosphorus (WP), on a pulsed high-energy laser (HEL) beam. An analysis of the aerosol (gaseous and particulate airborne material) was used as the basis for calculations of evaporative clearing, and application was made to a given specific test situation. Linear propagation properties forming the basis for the 10.6 μm pulsed laser nonlinear effects

DD FORM 1 JAN 73 1473 EDITION OF 1 NOV 65 IS OBSOLETE

410663

SECURITY CLASSIFICATION OF THIS PAGE (When Data Entered)

20. ABSTRACT (cont)

are obtained relatively directly by using spectrophone absorption and extinction, a light scatterng particle spectrometer and nephelometers (particle density as a function of radius and mass loading), and dew-point hygrometer (partial pressure of water vapor). General conclusions are that, for the smoke produced by burning WP, a CO_2 pulsed HEL beam clears the optical path quite rapidly and efficiently. The absorption after clearing is caused by the residual vapors and is much lower.

Accession For
NTIS GRA&I ☒
DTIC TAB ☐
Unannounced ☐
Justification

By
Distribution/
Availability Codes
Dist | Avail and/or Special
A

DTIC
ELECTE
JUL 2 1981
S D
D

RE: Classified Reference, Distribution Unlimited-
No change per Ms. Marie Richardson,
ASL/DELAS-DM-A

CONTENTS

LIST OF TABLES..... 4

LIST OF FIGURES..... 5

INTRODUCTION..... 7

MEASUREMENT SYSTEMS..... 7

AMBIENT ABSORPTION..... 9

AEROSOL CHARACTERIZATION FOR TESTS..... 16

EFFECT OF EVAPORATIVE CLEARING ON HIGH POWER BEAMS..... 25

CALCULATIONS, PART I: EVAPORATION OF SINGLE PARTICLES..... 28

CALCULATIONS, PART II: COLLECTIVE EFFECT..... 40

CONCLUSIONS..... 42

REFERENCES..... 44

APPENDIX A

CONSTANTS USED IN THE CALCULATIONS OF NONLINEAR EFFECTS..... 45

APPENDIX B

SAMPLE PULSE SHAPES..... 46

APPENDIX C

NEAR, NEAR FIELD BURN PATTERN..... 47

APPENDIX D

FAR FIELD PATTERN AT TARGET SITE FOR LASER CORRESPONDING TO NEAR FIELD BURN PATTERN OF APPENDIX C..... 48

APPENDIX E

METHOD OF ESTIMATING ENERGY DISTRIBUTION IN THE BEAM FOR S^3 LASER BEAM..... 49

APPENDIX F

HIGH-ENERGY SINGLE-PULSE PROPAGATION ESTIMATES..... 54

LIST OF TABLES

1. WP Characterization Instrumentation..... 7

2. Calculated Range of Gaseous Absorption Coefficients, α, in Trench (Pre-Smoke Test Values)..... 9

3. Definition of Symbols for Evaporative Clearing..... 27

4. Distribution of Energy in Far Field Beam Lobes for S^3 Laser..... 32

5. Parameters of Single Particle Clearing as Functions of Particle Size and Beam Lobe Number for E_{total} = 200 J and t_{pulse} = 3.2μs..... 34

6. Parameters of Clearing for Specific Conditions (Second Test) and Using Particle Radii of Peak Absorption..... 37

7. Parameters Showing Efficiency of Punch-Through for E_{total} = 40 J for Center Lobe..... 43

E-1. Calculation of Relative Intensities for S^3 Laser Beam Lobes..... 52

LIST OF FIGURES

1a. Major components of integrated field spectrophones..... 10

1b. Spectrophone calibration and gas flow setup..... 10

2. Spectrophone and nephelometer (right) on tripod..... 11

3. Spectrophone side of tripod mount..... 12

4. This view (just above that of figures 2 and 3) shows the MRI nephelometer control unit (rear) and PMS counter and dew-point hygrometer electronics in the foreground..... 13

5. Output recorders/printer..... 14

6. Spectrophone calibration setup in laboratory near site..... 15

7. Particle size distribution as a function of test time..... 17

8. Some temperatures and dew-point temperatures obtained during the first test..... 19

9. Growth of particles with relative humidity (smoke of phosphorus) 0.1μm to 10μm (radius) particles..... 19

10. Plot of measured complex indices for phosphoric acid at 10.6μmλ..... 19

11. Differential absorption for the first test..... 20

12. Absorption coefficient at 10.6μmλ for smoke of phosphorus during first test..... 21

13. Extinction coefficient as a function of time during the first test..... 23

14. Some temperatures and dew-point temperatures obtained during the second test..... 23

15. Absorption coefficient as a function of time for the second test..... 24

16. Illustration of large fluctuations in the absorption coefficient (2 s time resolution) early during the second test..... 24

17. Settling chamber measurements: nephelometer output relationship with extinction/absorption coefficients. Absorption coefficient = 0.96 x extinction coefficient..... 26

18. Absorption coefficient at the end of the second test, first by the center spectrophone and then by the center nephelometer..... 26

19. Sample real and approximate pulse forms..... 29

20. Expenditure of energy..... 30

21. Near, near field pattern..... 30

22. Far field pattern..... 31

23. Sketch of the double, double slit pattern..... 31

24. Illustration of relationship between laser pulse and propagation parameters..... 33

25. Time to evaporate center lobe in loaded aerosol medium. Loading given by absorption coefficient . E_{total} = 40.0 J (in lobe), R_p = 1μm, t_{pulse} = 3.2μs..... 41

26. Total energy transmitted in center spot as a function of absorption coefficient for the WP-smoke aerosol. No gaseous absorption effects included..... 42

E-1. S^3 laser output geometry..... 49

INTRODUCTION

In this report aerosol characterization measurements are analyzed for prediction of countermeasure aerosol effects on high-energy laser (HEL) beams. Although the general principles are applicable for various beam parameters, our calculations will be oriented toward those of a pulsed CO_2 laser (10.6μm wavelength) with a pulse length of about 3μs and a total beam energy of about 200 J. The focus of this effort will be the effect due to evaporative clearing. The basis for thermal blooming[1] (atmospheric lensing due to thermally created density gradients in the beam), the other major nonlinear effect, will be established by describing heating of the ambient gases and particles. Threshold calculations show that the 3μs pulse of these tests is short for strong blooming effects.

These measurements were performed in conjunction with a test of an HEL having the parameters described above. The beam traversed a trench approximately 100 m long. The trench was covered with polyethylene forming a relatively closed environment in which the smoke was dispersed and then measured as a function of settling time. Most of the characterization was performed at the midportions of the trench and assumed to approximate a spatial average since the smoke mixing, diffusing, and settling times were long at 1 to 2 h.

MEASUREMENT SYSTEMS

Table 1 lists the instrumentation used for the characterization.

TABLE 1. WP CHARACTERIZATION INSTRUMENTATION

Measurement	System	Manufacturer
Extinction absorption, coefficients at 10.6μm	CO_2 laser spectrophone	Atmospheric Sciences Laboratory (ASL)
Particle counting and sizing	Active cavity, light scattering particle spectrometer, HeNe	Particle Measurement systems (Model ASASP-X)
White light volume scattering coefficients	Nephelometer	Meteorological Research Instruments (Model 2050B)
Relative humidity and partial pressure of water vapor	Dew-point hygrometer, thermometer	Edgerton-Germehausen and Grier (Model 880)

[1] F. G. Gebhardt, 1976, "High power laser propagation," Appl Opt, 15(6):1479

The following paragraphs describe instruments and discuss the need for each type of information obtained.

Of the absorbing gaseous constituents at 10.6μm, water vapor is expected to be by far the strongest. The very high temperatures and dew points produced in the trench by the greenhouse effects resulted in relatively high partial pressures and thus high absorption coefficients. The Edgerton-Germehausen and Grier (EG&G) condensation plate dew-point hygrometer was used to obtain the water vapor partial pressures from which the water vapor absorption coefficients were computed. Relative humidity values obtained from the dew point and temperature data were used to compute fractional water content of the very hygroscopic smoke of burning phosphorus. This computation, in turn, was used to determine the appropriate complex refractive index and other physical properties of the smoke. Although site-peculiar gases are possible contributors, contributions to the net 10.6μm absorption coefficient due to other ambient gases can be reasonably estimated.

The distribution of particles with respect to size is important since the calculations of the nonlinear effects are also generally size dependent. The instrument used (ASASP-X) had been subjected to laboratory tests, first with particles of known sizes to determine accuracy in sizing and then with the smoke of phosphorus to determine response to high densities. Calibrations with respect to absolute density for each increment of particle radius are difficult to perform with accuracy and have not been accomplished for this instrument. As stated then, the form of the particle size distribution was the object of this measurement. The absolute magnitude of the absorption was obtained by using another technique--the spectrophone.

Before the measurements involving the spectrophone are discussed, an optical nephelometer measurement of aggregate particle scattering from within a given volume into a fixed solid angle will be introduced since it might be related to the net absorption. The nephelometer averages over a volume as does the spectrophone; but, like the particle measurement systems (PMS) instrument, it measures scattering. The calibration and use of a meteorological research instrument (MRI) type 2050B unit will be discussed later in this report.

The authors' application of spectrophones to atmospheric gases and particulates is documented in the literature.[2] In a more recent publication,[3] the authors discuss their spectrophone research on the smoke of white phosphorus (WP). Spectrophone theory has been documented,[4] [5] and a variety of ASL

---

[2]C. W. Bruce and R. G. Pinnick, 1977, "In-situ measurements of aerosol absorption with a resonant CW laser spectrophone," Appl Opt, 16:1762

[3]C. W. Bruce and Y. P. Yee, 1980, "In-situ measurement of the ratio of aerosol absorption to extinction coefficient," Appl Opt, 19:1893

[4]E. L. Kerr and J. G. Attwood, 1968, "The laser illuminated absorptivity spectrophone: A method for measurement of weak absorptivity in gases at laser wavelengths," Appl Opt, 7:915

[5]L. B. Kreutzer, 1971, "Ultralow gas concentration infrared absorption spectroscopy," Appl Phys, 42:2934

applications is described in an ERADCOM report.[6] The particular system used for these measurements was designed for field use and is tunable and stabilized for several 10um laser lines. Figure 1 shows a schematic cross section of this system, and figures 2 through 6 show on-site photographs of the instrumentation. The instrumentation was first mounted within the trench, but for the later data, the instrumentation was located outside and adjacent to the polyethylene cover, sampling within the trench through tubes.

AMBIENT ABSORPTION

The ambient gas and particulate absorption coefficients were measured before the tests. The particulate absorption was obtained indirectly by using particle counting results. Lorenz-Mie calculations were based on these data and complex refractive indices for soil-based (clay) dust. Though not really precise, this technique usually is accurate within a factor of three. The ambient level of particulate absorption (coefficient) was found to be approximately 10^{-3} km^{-1}. The total (gaseous and particulate) absorption coefficient as measured by the spectrophone was, as expected, much higher. Conditions within the trench were relatively repeatable from day to day. Typical parameters for calculations and calculated values are shown in table 2.

TABLE 2. CALCULATED RANGE OF GASEOUS ABSORPTION COEFFICIENTS, α, IN TRENCH (PRE-SMOKE TEST VALUES)

Date/ Time	Dew-Point Temperature (°C)	Partial Pressure (torr)	H_2O	α_{H_2O} (km^{-1})	α_{CO_2} @330 ppm (km^{-1})	α Total (minus trace gases) (km^{-1})
28-29 Jul 4-5 pm	80	26.2		0.66	0.08	0.74
30 Jul 5 pm	89.0	35.0		1.11	0.08	1.19
3 Aug 11 am	88.8	34.8		1.09	0.08	1.17

[6]Y. P. Yee, C. W. Bruce, and R. J. Brewer, 1980, Gaseous/Particulate Absorption Studies at WSMR Using Laser Sourced Spectrophones, ASL-TR-0065, US Army Atmospheric Sciences Laboratory, White Sands Missile Range, NM

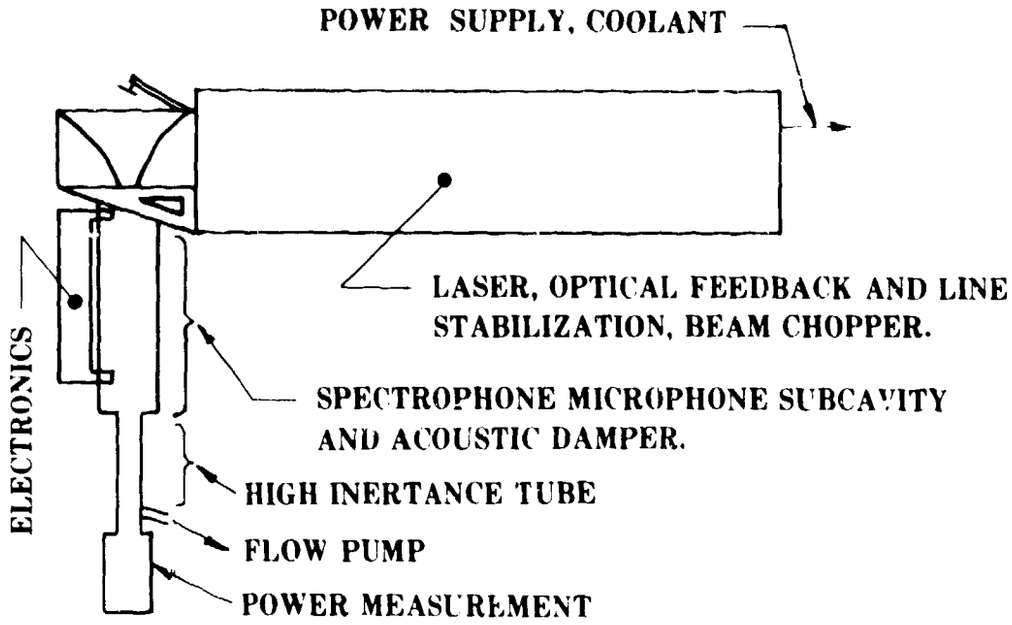

Figure 1a. Major components of integrated field spectrophones.

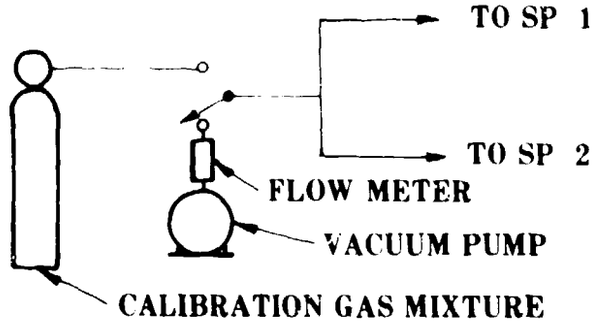

Figure 1b. Spectrophone calibration and gas flow setup.

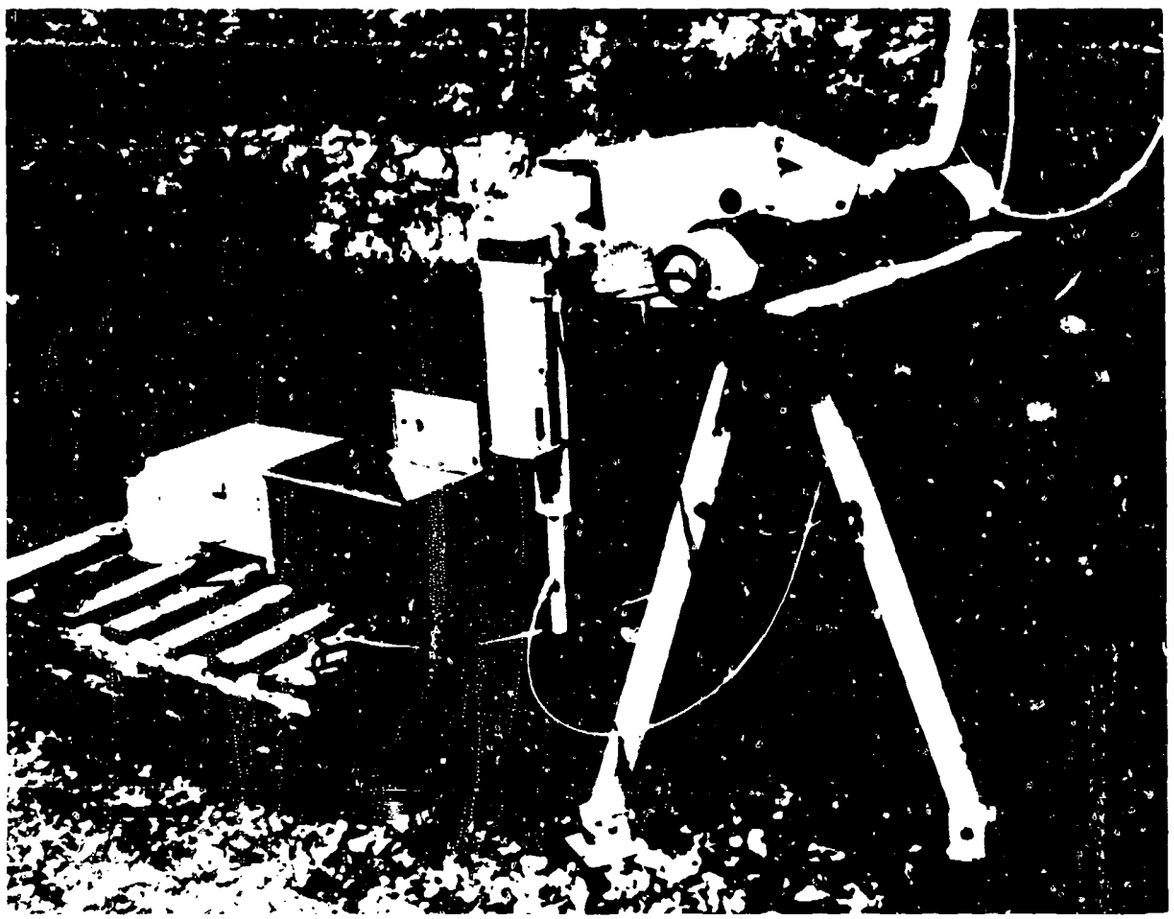

Figure 2. Spectrophone and nephelometer (right) on tripod.

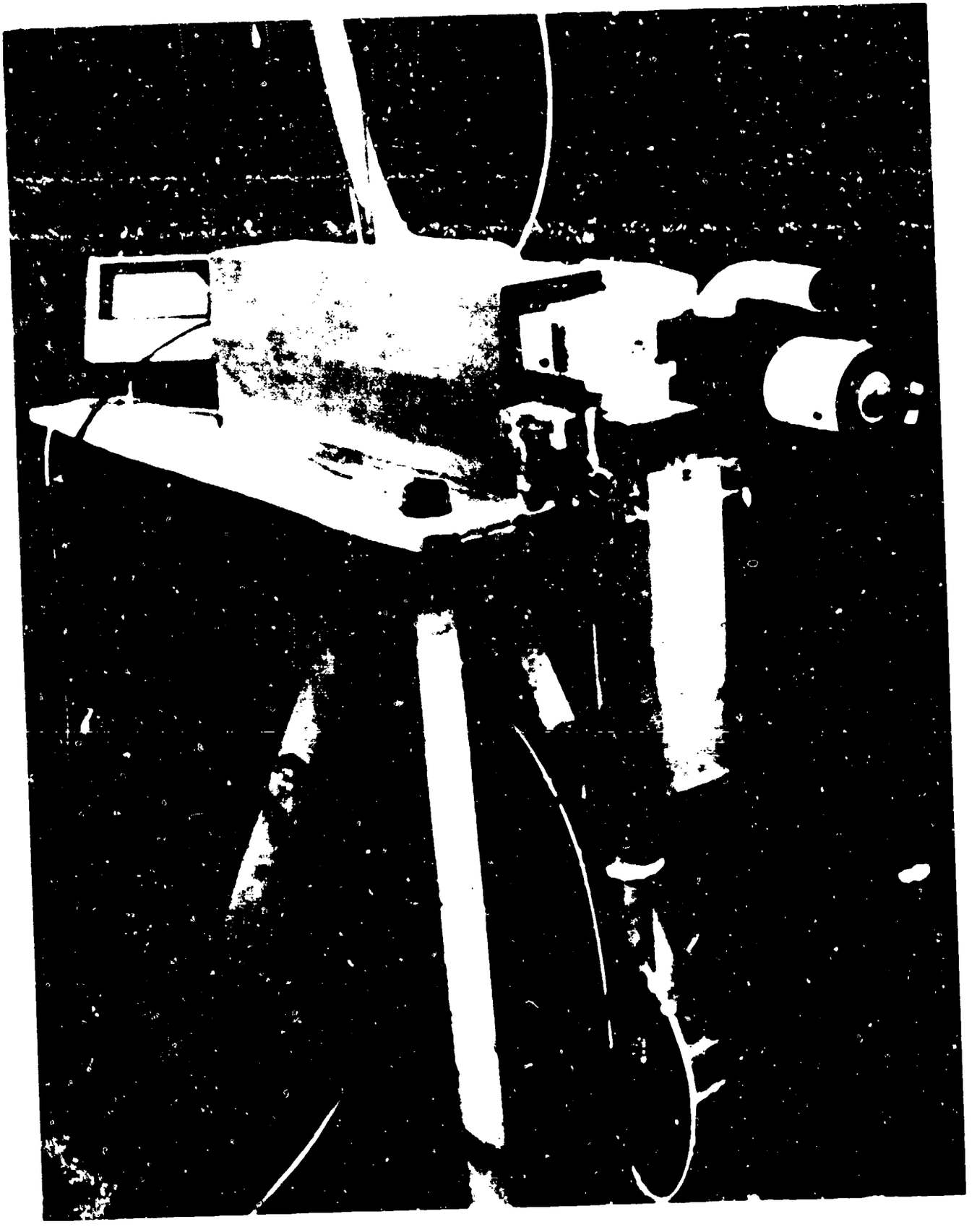

Figure 3. Spectrophone side of tripod mount.

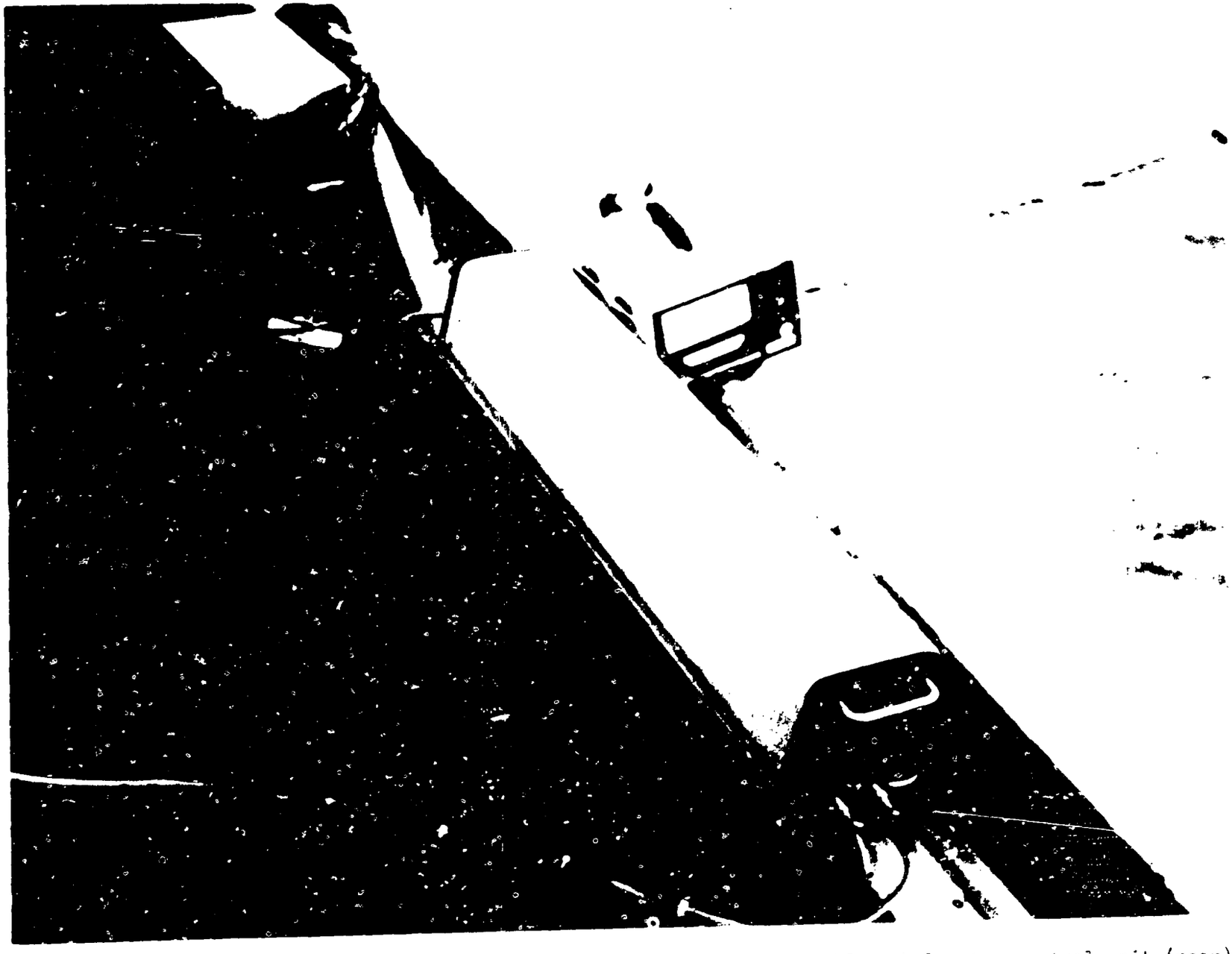

Figure 4. This view (just above that of figures 2 and 3) shows the MRI nephelometer control unit (rear) and PMS counter and dew-point hygrometer electronics in the foreground.

Figure 5. Output recorders/printer.

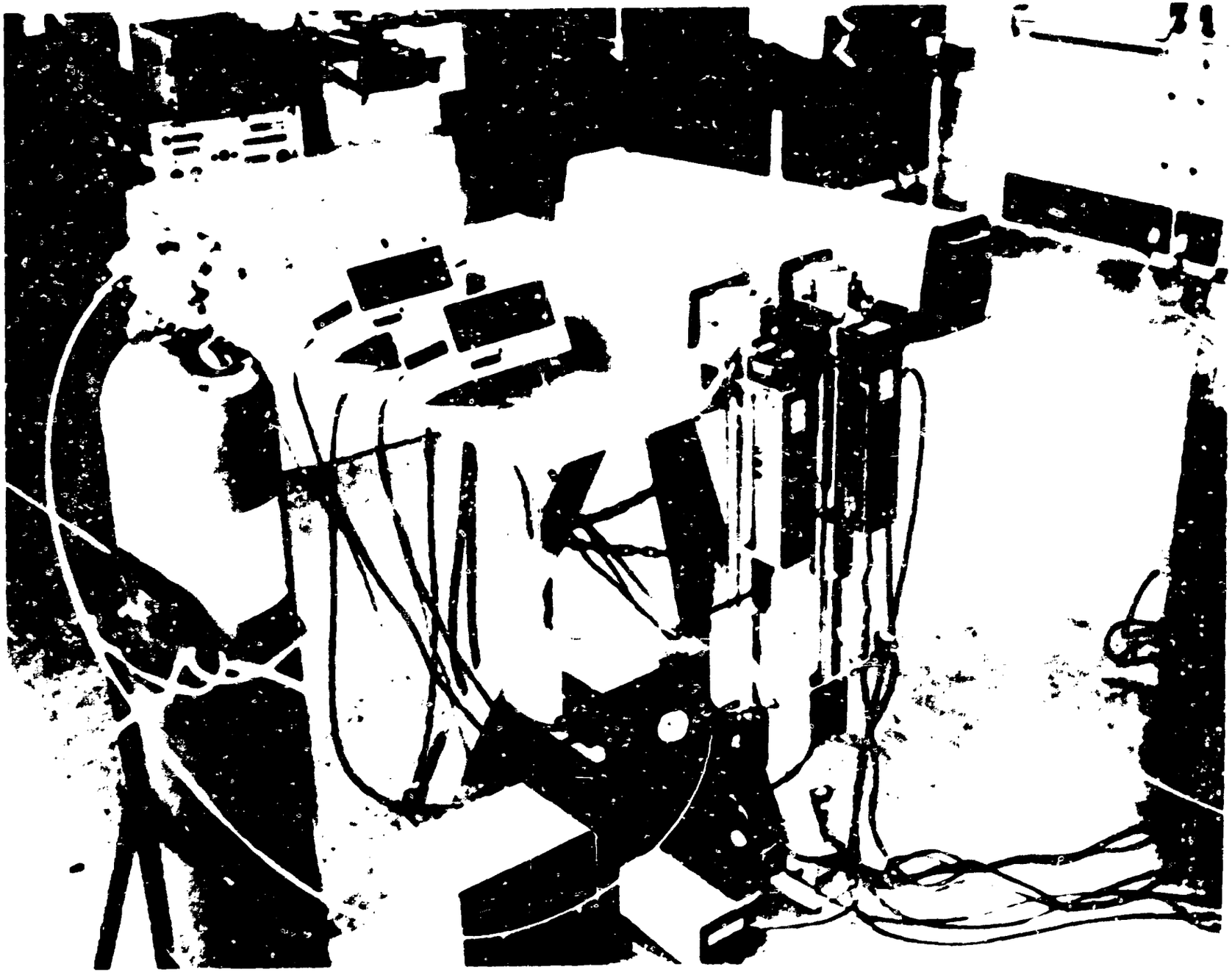

Figure 6. Spectrophone calibration setup in laboratory near site.

The partial water pressure was based on extrapolations from the data of Yin et al,[7] and the results were based on data of Shumate et al,[8] about 11 percent lower for these partial pressures. One tunnel section (within 4 m of the measurements) was removed for the 28-29 August, 4 to 5 pm times. The section cover was reinstalled before the aerosol tests, and the data here for 30 July and 3 August are for completely covered trenches.

The measured gaseous absorption coefficient corresponding to the first example (data of 28-29 July 1980) was 1.1 km^{-1}. Probable error figures on this measurement are not precise but are estimated to be 0.2, largely because of temporal variations due to unknown source(s). Higher than predicted values of the absorption coefficient frequently occur in ASL field measurements of ambient absorption at 10μm wavelengths.

Absorption due to trace constituents could elevate the value considerably. A rough rule of thumb is that trace gas absorption (within an absorption band region) often reaches or exceeds 1 $(ppm\text{-}km)^{-1}$ and, of course, 1 ppm is not a high concentration.

During the measurement program, test project personnel frequently mentioned the desire to obtain total absorption values lower than those measured or predicted (minus trace gas contributions). Another reason for interest in the ambient gaseous absorption is that the smoke aerosol level approached these levels near the end of each test.

AEROSOL CHARACTERIZATION FOR TESTS

Aerosol characterization for two test situations will be discussed. The dates and approximate starting times are listed as the latter two examples in table 2 (information for 30 July 1980 and 3 August 1980). The most notable difference in the conduct of these two tests is the time of day. Aerosol characteristics were similar, in the mean.

The procedure was to ignite phosphorous smoke grenades in the trench at about the one-quarter and three-quarter length positions. The smoke dispersed roughly over a 2-h period during which aerosol measurements were made. The data and analyses will be presented as functions of the evolving aerosol system and implications for nonlinear effects will be discussed.

Particle size distribution evolved generally as expected from prior laboratory measurements on the same aerosol; that is, the mean densities decreased and the peak moved to progressively smaller sizes. Figure 7 shows a composite graph of the distribution pattern for the first test. These data represent roughly 1-min averages (data were not always continuously available in time). Circulation under the loosely fit trench cover (and pumping action by

---

[7]P. K. L. Yin and R. K. Long, 1968, "Atmospheric absorption at the line center of P(20) CO_2 laser radiation," Appl Opt 7:1551

[8]M. S. Shumate et al, 1976, "Water vapor absorption of carbon dioxide laser radiation," Appl Opt 15:2480

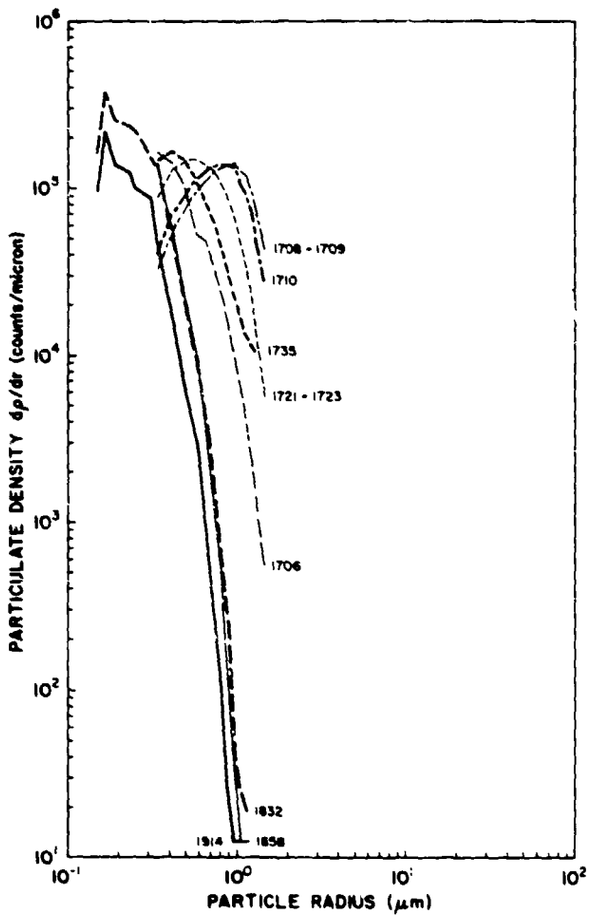

Figure 7. Particle size distribution as a function of test time.

fluctuations in air pressure on top of the plastic cover) was sufficient that any type of settling calculations to determine decreasing densities would be questionable.

The differential absorption coefficients (absorption per micrometer particle radius) were calculated by using Lorenz-Mie theory with optical constants appropriate to the composition of the smoke. To accomplish this calculation, the relative humidity for the test was computed from the measurements of figure 8. The relative humidity was used in turn to calculate the percent of water for the hygroscopic smoke on the basis of measurements made in our laboratory and also predicted by the theory of Hanel and Bullrich.[9] The relationship is plotted in figure 9. Finally, the complex indices were obtained from a work by Querry and Tyler,[10] but their data posed a problem; two sets of complex indices were obtained from this source (figure 10). We have discussed the strange appearing results with the authors who maintain that both sets are correct. We have simply used them (no measurements fell in the disjointed data gap).

Figure 11 represents a plot of the differential absorption based on the data of figure 7. The absorption peak occurs at a radius of about 1.2μm soon after the smoke is dispersed and decreases relatively smoothly to about 0.4μm in roughly 2 h; in the same time the peak absorption level has dropped roughly two orders of magnitude. At the midpoint in this 2-h evolution, 80 percent of the absorption occurs within a radius span of approximately 0.30μm.

The background particulate absorption is represented by the lowest curve labeled 1641, that is, before the smoke was released. The contribution here (at about 10^{-3}km^{-1}) is well below the ambient gaseous absorption.

The total absorption coefficient as calculated from the particle size and density information is plotted as a function of time in figure 12. For this presentation, 1-min averages obtained at approximately 10-min intervals are connected by straight-line segments. These values are much lower than those of the spectrophone measurements. The spectrophone yielded absorption and extinction coefficient peak values (in separate measurements) of about 200 and 220 km^{-1}, while the particle counter result was about 10 km^{-1}. This difference is believed to be due primarily to low counting efficiencies and sampling errors in unknown proportions. As the purpose of sizing and counting for these tests was to obtain measurements of the form of the size distribution as a function of time rather than absolute values, this difference is not a problem. Prior calibration of the counter using monodisperse aerosols precludes sizing as a prime source of error. Likewise, the optical constants and calculational scheme introduce uncertainties that are very small compared with the difference.

---

[9]G. Hanel and K. Bullrich, 1978, "Physico-chemical property models of tropospheric aerosol particles," Beitrage Zur Physik der Atmosphare, 51:129

[10]M. R. Querry and I. L. Tyler, 1978, "Complex refractive indices in the infrared for H_3PO_4 in water," J Opt Soc Am, 68:1404

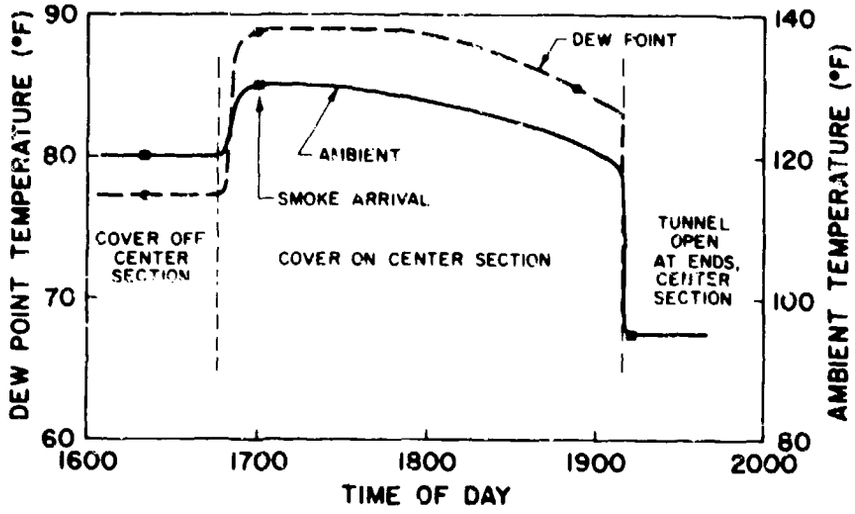

Figure 8. Some temperatures and dew-point temperatures obtained during the first test.

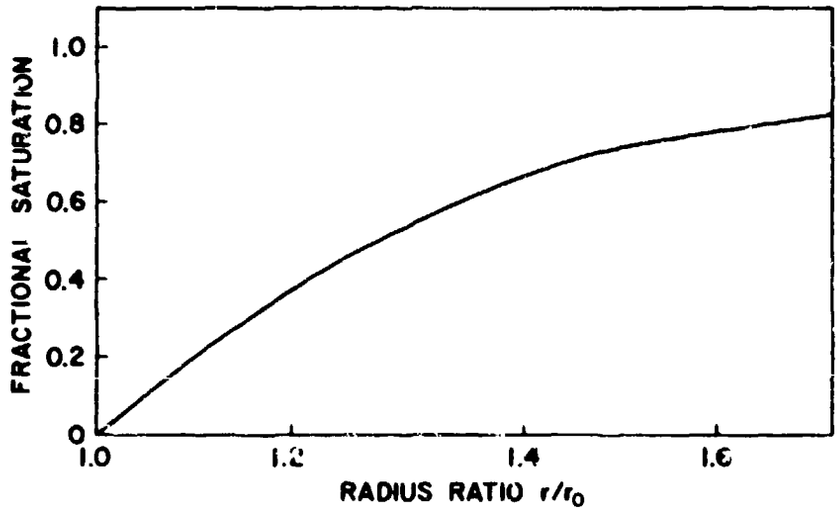

Figure 9. Growth of particles with relative humidity (smoke of phosphorus) 0.1μm to 10μm (radius) particles.

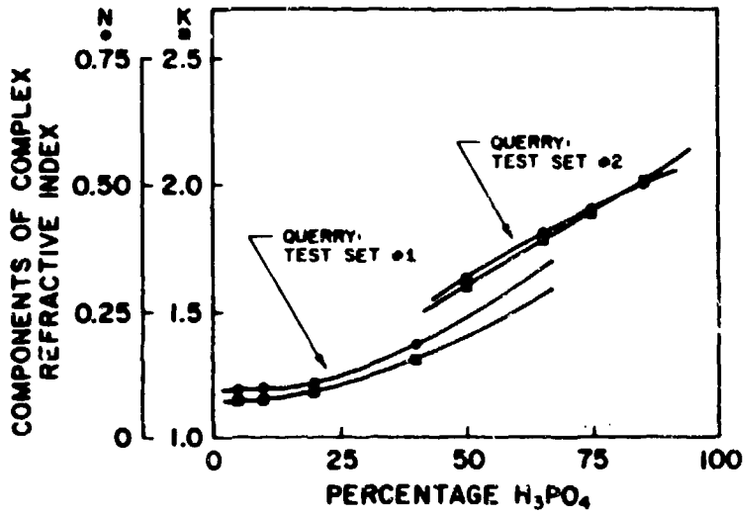

Figure 10. Plot of measured complex indices for phosphoric acid at 10.6μmλ.

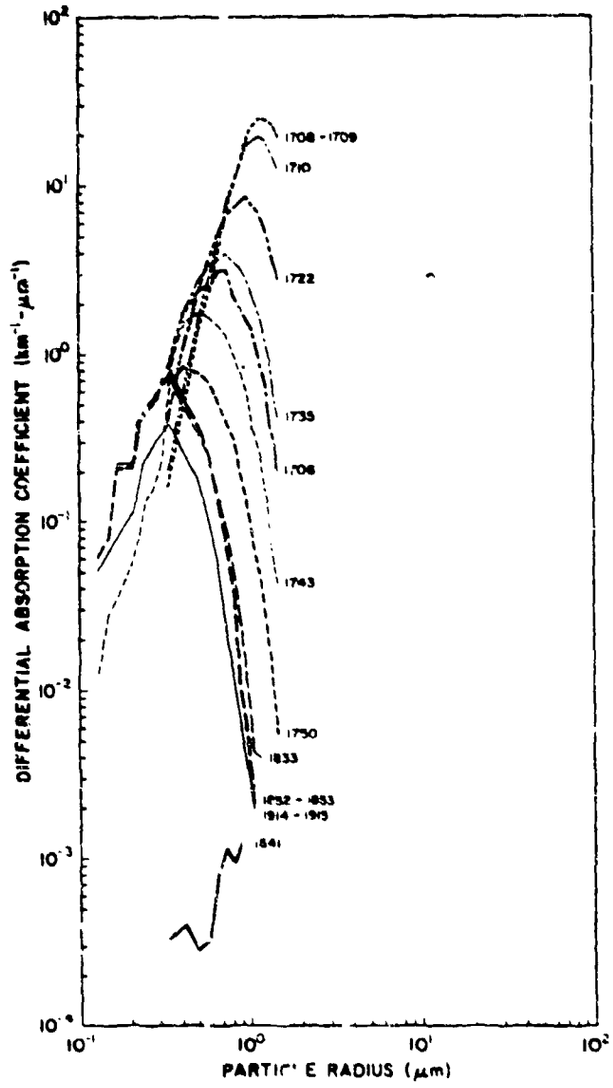

Figure 11. Differential absorption for the first test.

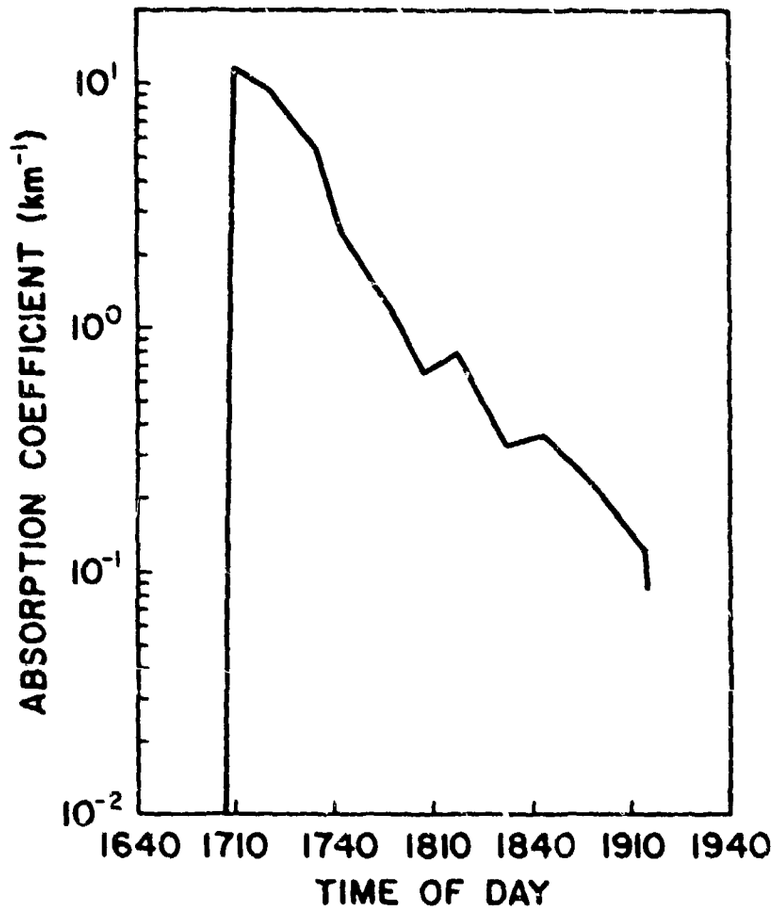

Figure 12. Absorption coefficient at 10.6μmλ for smoke of phosphorus during first test.

A comparison of figures 7 and 11 shows that the largest size particles are most important in the calculation of the total absorption because of the rapid increase with particle radius of the Lorenz-Mie efficiency factor for the absorption cross section. Therefore, the apparent increase with time in the densities of the relatively small particles (whose signals are probably masked in the counter by those from the larger particles) is not of concern here. A designed-in characteristic of the counter is also partly at fault in this misrepresentation which causes a "tailing-off" effect in the signals representing progressively smaller sizes.

Calculations to follow are based on the peak absorption values which agree well with the author's predictions based on the laboratory measurements of reference 3 (within 15 percent).

The measurement of extinction coefficient derived from power loss in the spectrophone is satisfactory at high values (early in the test) but is not useful below 10 km^{-1} due to the question of power meter drift. Figure 13 shows the extinction coefficient for the test of figure 12. The slope of the decreasing extinction coefficient with time, however, agrees well with that found by using the PMS particle counter data. An electronic problem, presumed to be overheating of system electronics prevents complete comparison of spectrophone absorption data for this test.

Time variations culled from the extinction, the density distribution, and the absorption measurements at the location of the apparatus were greater than a factor of five for integration times less than 3 s and about a factor 2 to 3 for integration times of 10 s. However, a spatial density average over as much as 10 percent or greater volume of the trench probably varies less than 20 percent.

The temperature time series for the second test is given by figure 14.

Temperatures in the trench were somewhat lower than the temperatures in the first test even though the second tests were during midday (the 30 July test was later in the afternoon). Particle size distributions and their evolution in time were similar in form though the corrosive action of the smoke caused a reduction in particle counter laser power for this test. The spectrophone measured peak absorption and extinction values were virtually the same at 200 km^{-1}. Absorption coefficient as a function of time for this test is shown in figure 15. For a resolution time of about 2 s, the magnitude fluctuates by more than an order of magnitude (figure 16). The same data, when averaged over about a minute for each of the sampling periods, yield a much more steady decrease. This decrease has nearly the same mean slope as that calculated from the particle counter data though the magnitudes are very different.

In contrast to the spectrophone, the nephelometer measurement yields primarily particle scattering information (molecular scattering is generally much lower). Due to their high sensitivity, data were obtained only at the very end of these tests--when the ends of the trench were opened near test completion. The nephelometer output (scattering coefficient at visible wavelengths)

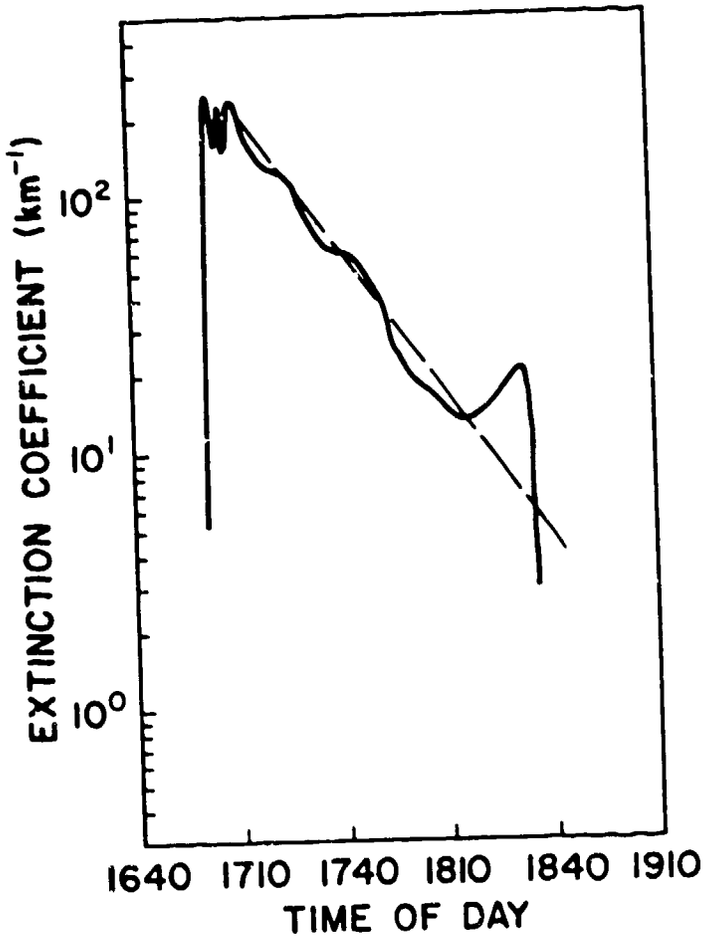

Figure 13. Extinction coefficient as a function of time during the first test.

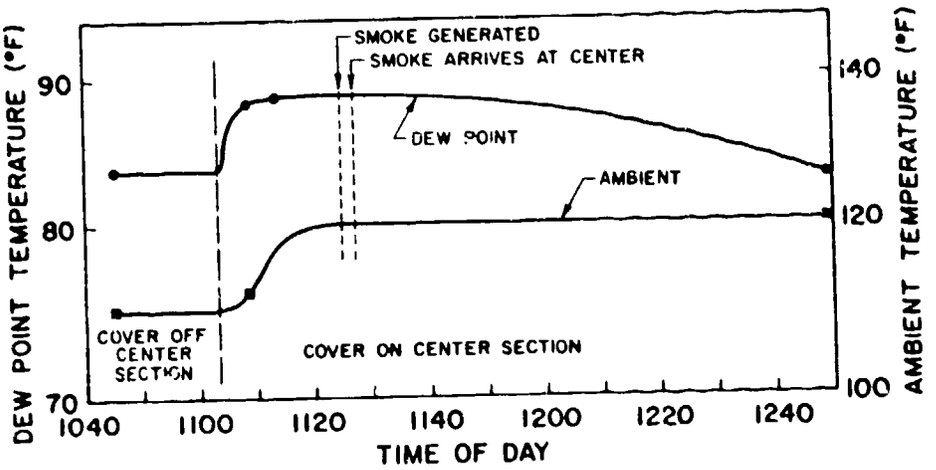

Figure 14. Some temperatures and dew-point temperatures obtained during the second test.

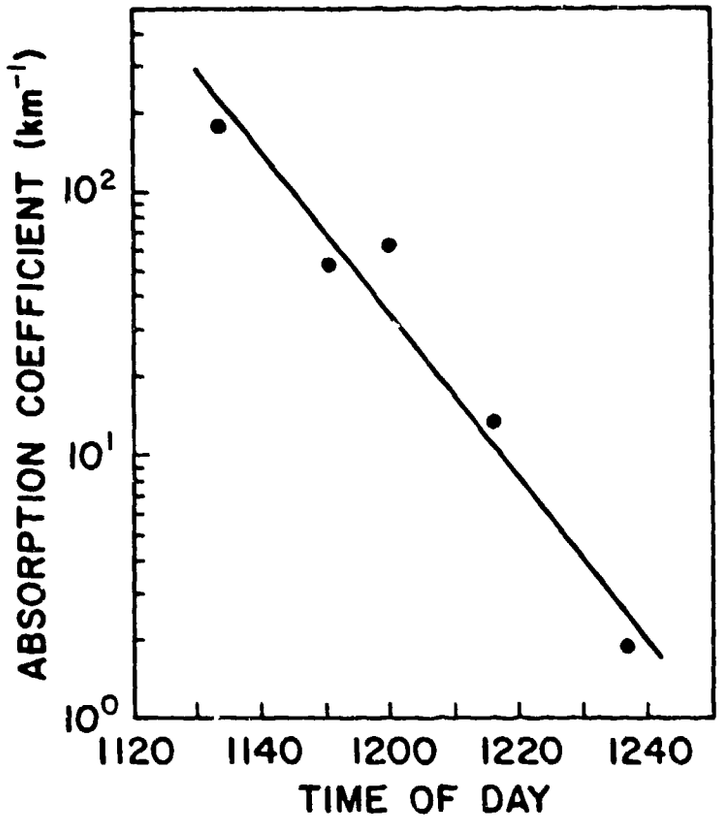

Figure 15. Absorption coefficient as a function of time for the second test.

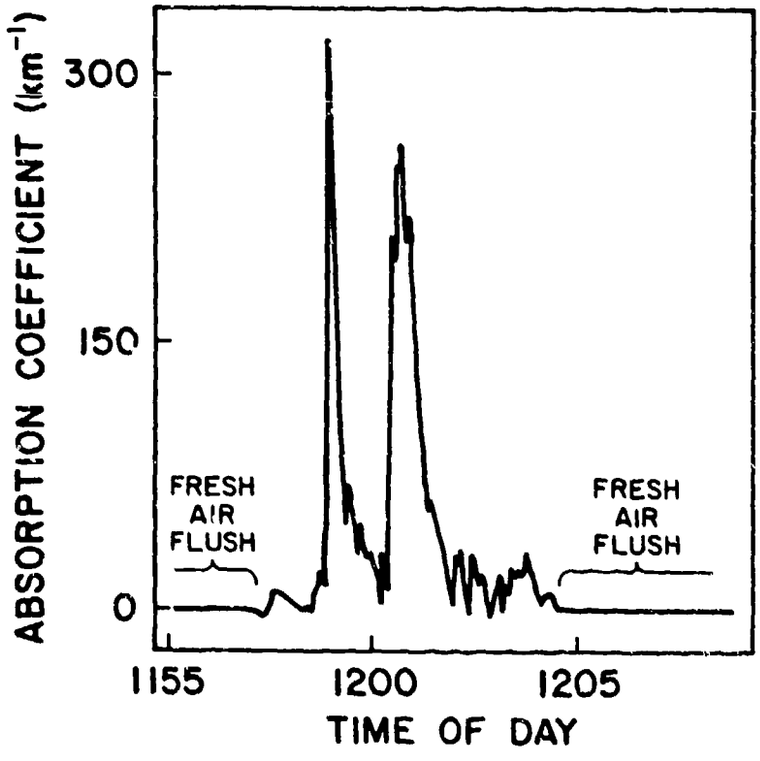

Figure 16. Illustration of large fluctuations in the absorption coefficient (2 s time resolution) early during the second test.

was related in a laboratory calibration to extinction and absorption coefficients at a wavelength of 10.6μm (figure 17). Since there was no evidence of nonlinearity, a single constant serves to relate the volume scattering coefficient to extinction, that is, $\left[\frac{1}{6} \frac{km^{-1}}{Sc. Coef.}\right]$ and another to relate the scattering coefficient to absorption $\left[0.96 \times \frac{1}{6} \frac{km^{-1}}{Sc. Coef.}\right]$ for the smoke of WP.

Figure 18 shows how the particulate concentration can fall at the center position when the wind is allowed to flush the trench. A nephelometer near the target end of the trench (about 6 m from the end), though, recorded that the fluctuating smoke attenuation decreased in that region rapidly to below 2 km^{-1} at about 1218, while near the center, the absorption coefficient level was still near 10 km^{-1}. For about 1 min during which laser pulse 7718 was fired through the trench (1214 to 1215), this nephelometer measured $\alpha = 1.51 \pm 0.06\ km^{-1}$.

The smoke of WP is hygroscopic, quickly drawing water from the vapor state. The reduction of the relative humidity resulting from the introduction of the smoke into the tunnel was calculated on the basis of prior laboratory measurements, that is, a smoke production efficiency factor of $k_E = 0.35\ m^2/gm$ and a fractional growth in particle radius of $r/r_0 = 1.21$ for an initial relative humidity of 35 percent.[9] By using the initial value of absorption to calculate the mass density of the smoke ($\rho_m = 0.16\ gm/m^3$) and assuming a dew-point temperature of 84°F to obtain the initial partial pressure of water (29.8 torr), a partial pressure change of less than 0.1 torr was obtained. This change is negligible for effects of interest here.

EFFECT OF EVAPORATIVE CLEARING ON HIGH POWER BEAMS

The tendency to punch-through the absorbing countermeasure aerosol WP is of prime interest here, and parameters from the two similar tests will be used as a basis. The thermodynamic and optical bases for the calculations will be applied by using laser beam parameters relevant to a system whose beam parameters are to be described (US Army Missile Command [MICOM] S^3 system).

---

[9]G. Hanel and K. Bullrich, 1978, "Physico-chemical property models of tropospheric aerosol particles," Beitrage Zur Physik der Atmosphare, 51:129

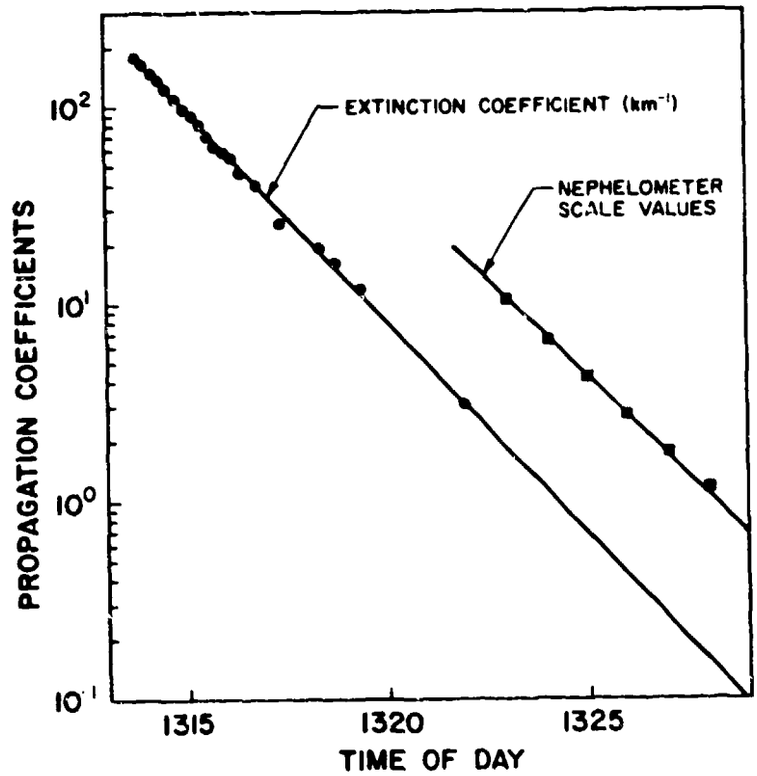

Figure 17. Settling chamber measurements: nephelometer output relationship with extinction/absorption coefficients. Absorption coefficient = 0.96 x extinction coefficient.

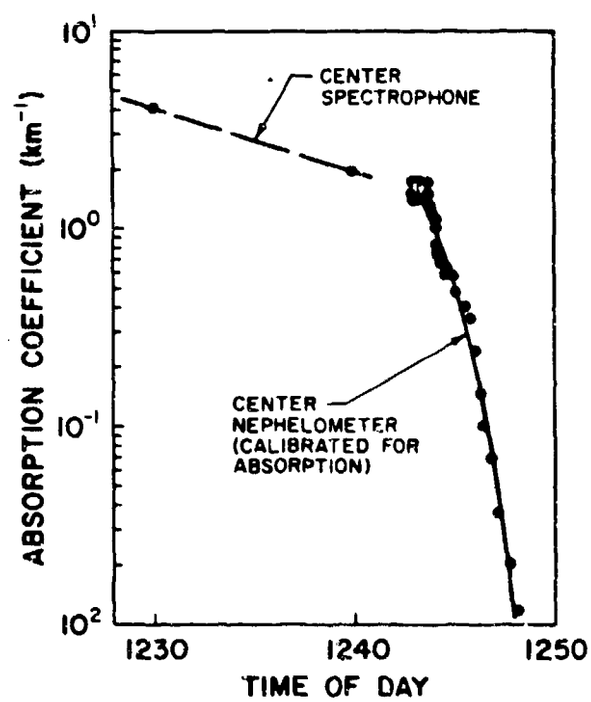

Figure 18. Absorption coefficient at the end of the second test, first by the center spectrophone and then by the center nephelometer.

The thermodynamical calculations for the clearing effect begin with the dictionary of terms listed in table 3. Glickler[11] and Sutton[12] used elaborate (but still inexact) integral solutions to describe clearing by fog.

TABLE 3. DEFINITION OF SYMBOLS FOR EVAPORATIVE CLEARING

Q	-	heat (joules)
R_p	-	radius of particle (micrometers, centimeters)
R_B	-	radius of beam (centimeters)
r	-	variable representing radius
P	-	instantaneous power (watts)
E	-	beam energy (joules)
ρ_m	-	bulk density of particulate material (grams/cubic centimeters)
c	-	specific heat of particulate material (joules/grams degrees Kelvin)
H	-	latent heat of vaporization (joules/grams)
$Q_\alpha - Q_\varepsilon$	-	Lorenz-Mie efficiency factors for absorption and extinction
T	-	mean temperature of particle (degrees Kelvin)
t	-	time (seconds)

Note that ρ_m, c, T_{Boil}, H, and the complex refractive indices leading to Q_α and Q_ε are functions of the relative humidity. The values are listed in appendix A.

[11] S. L. Glicker, 1971, "Propagation of a 10.6μm laser through a cloud including droplet vaporization," Appl Opt, 10:644

[12] G. W. Sutton, 1978, "Fog hole boring with pulsed high energy lasers: An exact solution including scattering and absorption," Appl Opt, 17:3424

CALCULATIONS, PART I: EVAPORATION OF SINGLE PARTICLES

Particles are first heated to boiling T, assuming spatially uniform heating of the particle, and then energy is added to evaporate them.

To reach boiling temperature, the rate of heating,

$$Q = \pi R_p^{\,2} Q_\alpha \left[\frac{P}{(\pi R_B^{\,2})} \sim \text{beam power density} \right]$$

then is integrated, $Q = \left(\frac{R_p}{R_B}\right)^2 Q_\alpha \int_0^t P dt$, and equated with the energy required to boil the particle.

$$Q = \frac{4}{3} \pi R_p^{\,3} \rho_m c \Delta T \ .$$

Now $\int_0^{t'} P dt$ is just the energy, E, which has passed the plane of the particle considered (to time t'). Solving for this energy, one obtains

$$E_B = \left(\frac{4\pi}{3}\right) \frac{\rho_m R_p R_B^{\,2} c}{Q_\alpha} \Delta T \ .$$

To add the heat of vaporization,

$$E_{LHV} = \left(\frac{4\pi}{3}\right) \frac{\rho_m R_p R_B^{\,2}}{Q_\alpha} H \ .$$

The sum of these two processes represents the total beam energy which has passed the plane of a particle of radius R_p at the time of evaporation, that is,

$$E_{cum}(R_p) = E_B(R_p) + E_{LHV}(R_p)$$

An examination of the S^3 laser pulse intensity profiles led to the suggestion that the pulse be modeled as triangular in time.* Samples pulse shapes are shown in appendix B. Figure 19 shows sample real and approximate pulse forms.

---

*Bill Jones, MICOM, private communication

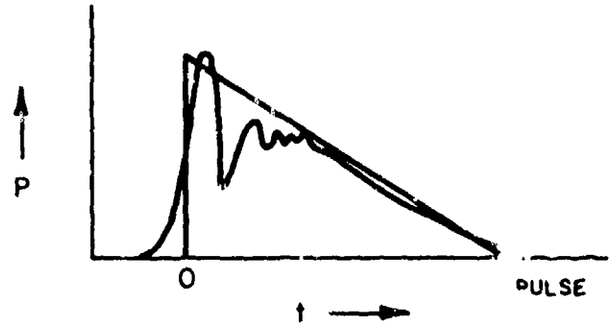

Figure 19. Sample real and approximate pulse forms.

Sample (and typical) parameters are

$E_{(total)}$ = joules

t_{pulse} = 3.2μs

P_{max} = 125 mW

The objective here is to determine the time to evaporate particles and then to calculate the energy remaining for each power lobe of the far field pattern.

$$E_{cum} = \int_0^{t'} P dt \ .$$

Then using a linear form

$$E_{cum} = \int_0^{t'} (mt + P_{max}) dt$$

$$= \frac{m}{2} (t')^2 + P_{max} t' \text{ where } m = -\frac{P_{max}}{t_{pulse}}$$

Solving this for t', the cumulative pulse time,

$$t' = t_{pulse} - \sqrt{t_{pulse}^2 - \left(2\,\frac{E_{cum}}{P_{max}}\right)\left(t_{pulse}\right)}\,.$$

Here it is assumed that the particle is vaporized and vaporous at time t'. The first simplifying assumption is justified since clearing is effective when particle diameters are reduced in boiling by considerably less than an order of magnitude (see figure 11). The second assumption follows from kinetic calculations showing that dispersal velocities are sufficient to form an effective vapor state within an interval very short compared with the pulse duration.

Figure 20 shows the problem schematically.

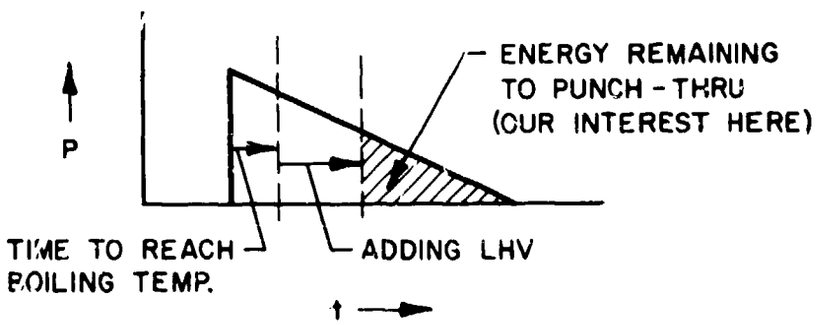

Figure 20. Expenditure of energy.

Now the energy (or power) density distribution in the beam must be determined.

The job is simplified since the laser output is a line-square, that is, two pairs of parallel slits in orthogonal directions (figure 21). A sample burn pattern (quite overburned) is shown in appendix C.

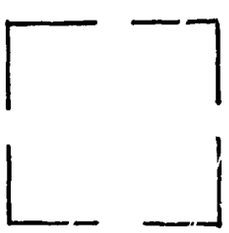

Figure 21. Near, near field pattern.

The power densities in the near, near field are therefore those of orthogonal pairs of finite slits and, in the far field, are the combined diffraction patterns of these slits. Actual burn patterns (sample in appendix D) look quite like the sketch of figure 22.

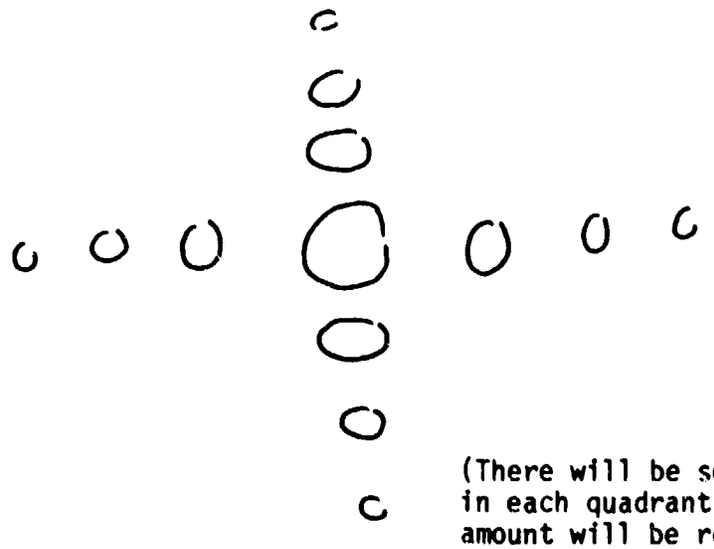

(There will be some energy in each quadrant, but the amount will be relatively small compared with the identified energy "lobes.")

Figure 22. Far field pattern.

The approach is to estimate the distribution of energy in this pattern or that in the area under the twin slit intensity profile.

$$I \sim \left(\frac{\sin^2\beta}{\beta^2}\right) x \left(\cos^2 \alpha\right) ,$$

that is, the single slit pattern (first term) modulated by that of the twin slits. Beta and alpha contain the viewing angle and dimensional parameters of the calculation.

Figure 23 shows a perspective sketch of the far field beam profile.

Figure 23. Sketch of the double, double slit pattern

$$P \cong K\Sigma I_i a_i \approx Ka\Sigma_i I_i \ ,$$

where I_i are the relative intensities and the K is found from the total energy and the pulse shape.

Appendix E contains the details of the calculation of the distribution of energy in the laser beam to which this formula is applied.

The distribution of energy in the lobes as calculated in appendix E is given in table 4.

TABLE 4. DISTRIBUTION OF ENERGY IN FAR FIELD BEAM LOBES FOR S^3 LASER

Lobe* Number	Percent E per Lobe	Percent E per Lobe / Lobe Area (cm^{-2})	Energy Density per Lobe for E_{total} = 200 J (J/cm^2)
0	18.7	7.19	14.4
1	8.5	4.47	8.94
2	6.3	3.32	6.64
3	3.7	1.95	3.90
4	1.5	0.79	1.58
5	0.3	0.16	0.32

*Increasing away from center

The total area involved at the target distance is approximately 40.6 cm^2.

The clearing time and then the fractional energy remaining to be transmitted after clearing will be calculated. The clearing time and fractional energy will then be obtained for the entire beam.

The clearing process effectively reduced the absorption to gaseous levels which are much lower, that is, to near normal atmospheric levels. The scattering is, of course, also greatly reduced; however, for the smoke of WP, the fraction of CO_2 laser beam energy scattered to that absorbed is less than 10 percent. The atmospheric propagation is therefore related to the punch-through effect in a form illustrated in figure 24.

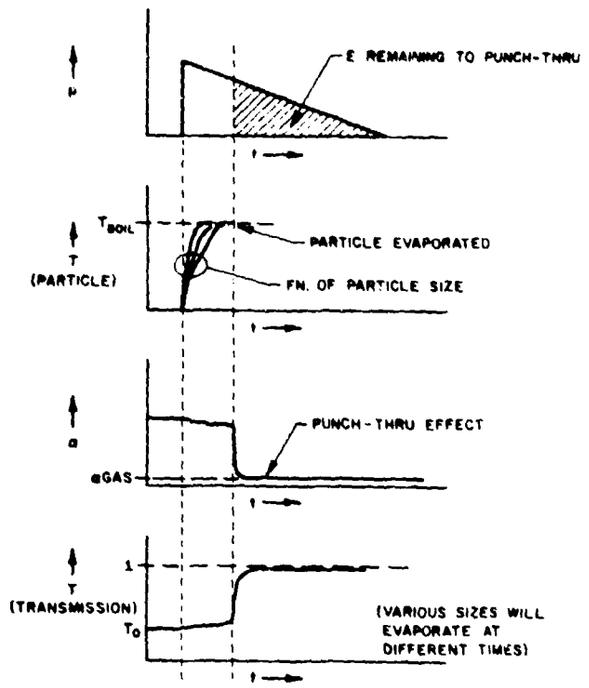

Figure 24. Illustration of relationship between laser pulse and propagation parameters.

Tables 5 and 6 show rapid and effective clearing as a function of smoke particle size for a relative humidity of 35 percent. Earlier data show that very few particles are larger than $R_p \simeq 4\mu m$ and that the clearing efficiency is almost independent of size to that point because of the increase in Lorenz-Mie efficiency with radius (up to $R_p = 4\mu m$) in spite of the growing mass to be evaporated. Coincidentally, this convenient independence disappears for the larger particles. The last column represents the efficiency of punch-through or, in other words the percentage of energy in the cleared field. The transmission is not unity at that point (as was mentioned) but reverts nearly to the pretest levels.

TABLE 5. PARAMETERS OF SINGLE PARTICLE CLEARING AS FUNCTIONS OF PARTICLE SIZE AND BEAM LOBE NUMBER FOR E_{TOTAL} = 200 J AND T_{PULSE} = 3.2μs.

Center Lobe (0)
Energy = 40.0 J

R_p (μm)	Q_α	Time to Evaporate (μs)	Fraction of Energy in Remaining Portion of Pulse
0.01	0.00202	1.68×10^{-1}	0.90
0.05	0.0101	1.68×10^{-1}	0.90
0.10	0.0203	1.67×10^{-1}	0.90
0.15	0.0305	1.67×10^{-1}	0.90
0.20	0.0511	1.32×10^{-1}	0.92
0.40	0.0828	1.64×10^{-1}	0.90
0.60	0.127	1.60×10^{-1}	0.90
1.0	0.222	1.52×10^{-1}	0.91
2.0	0.490	1.38×10^{-1}	0.92
4.0	0.904	1.50×10^{-1}	0.91
8.0	1.217	2.25×10^{-1}	0.87
10.0	1.265	2.72×10^{-1}	0.84
15.0	1.2600	4.20×10^{-1}	0.76
20.0	1.2123	6.00×10^{-1}	0.66
25.0	1.1663	8.09×10^{-1}	0.56
30.0	1.1663	1.01	0.47
40.0	1.1663	1.47	0.29
50.0	1.1663	2.11	0.12
60.0	1.1663	>3.2	0.00

TABLE 5. (Cont)

First Side Lobe (1)
Energy = 18.1 J

R_p (μm)	Time to Evaporate (μs)	Fraction of Energy in Remaining Portion of Pulse
0.01	2.76×10^{-1}	0.83
0.05	2.76×10^{-1}	0.83
0.10	2.75×10^{-1}	0.84
0.15	2.74×10^{-1}	0.84
0.20	2.16×10^{-1}	0.87
0.40	2.69×10^{-1}	0.84
0.60	2.63×10^{-1}	0.84
1.00	2.50×10^{-1}	0.0
2.00	2.26×10^{-1}	0.0
4.00	2.46×10^{-1}	0.0

Second Side Lobe (2)
Energy = 13.5 J

0.01	3.77×10^{-1}	0.78
0.05	3.77×10^{-1}	0.78
0.10	3.77×10^{-1}	0.78
0.15	3.77×10^{-1}	0.78
0.20	2.94×10^{-1}	0.82
0.40	3.67×10^{-1}	0.0
0.60	3.58×10^{-1}	0.0
1.00	3.41×10^{-1}	0.0
2.00	3.07×10^{-1}	0.0
4.00	3.34×10^{-1}	0.0

TABLE 5. (Cont)

Third Side Lobe (1)
Energy = 7.88 J

R_p (μm)	Time to Evaporate (μs)	Fraction of Energy in Remaining Portion of Pulse
0.01	6.75×10^{-1}	0.62
0.05	6.75×10^{-1}	0.62
0.10	6.75×10^{-1}	0.62
0.15	6.75×10^{-1}	0.62
0.20	5.20×10^{-1}	0.70
0.40	6.57×10^{-1}	0.0
0.60	6.41×10^{-1}	0.0
1.00	6.07×10^{-1}	0.0
2.00	5.44×10^{-1}	0.0
4.00	5.95×10^{-1}	0.0

Fourth Side Lobe
Energy = 3.20 J

0.01	2.37	0.69×10^{-1}
0.05	2.37	0.69×10^{-1}
0.10	2.37	0.69×10^{-1}
0.15	2.37	0.69×10^{-1}
0.20	1.56	0.26
0.40	2.04	0.91×10^{-1}
0.60	2.14	0.0
1.00	1.95	0.0
2.00	1.66	0.0
4.00	1.89	0.0

(Particles in the fifth side lobe require > 3.2μs)

TABLE 6. PARAMETERS OF CLEARING FOR SPECIFIC CONDITIONS (SECOND TEST) AND USING PARTICLE RADII OF PEAK ABSORPTION

Time: 1159

Run Number 7716

t_{max} = 3.0μs

E_{total} = 144.9 J

R_p = 1.0μm

Q_α = 0.2217

Beam Lobe Number (from center)	P_{max} (W)	Time to Boil and Evaporate (μs)	Fraction of Energy in Remaining Portion of Pulse
0	1.81×10^7	2.12×10^{-1}	0.86
1	8.21×10^6	3.50×10^{-1}	0.78
2	6.09×10^6	4.83×10^{-1}	0.70
3	3.57×10^6	8.90×10^{-1}	0.49
4	1.45×10^6	>3.0	0.0
5	2.90×10^5	>3.0	0.0

Time: 1203

Run Number 7717

t_{max} = 4.1μs

E_{total} = 212.5 J

R_p = 1.0μm

Q_α = 0.2217

0	1.94×10^7	1.95×10^{-1}	0.91
1	8.81×10^6	3.20×10^{-1}	0.85
2	6.53×10^6	4.38×10^{-1}	0.80
3	3.84×10^6	6.69×10^{-1}	0.63
4	1.55×10^6	2.52×10^{-1}	0.16
5	3.11×10^5	>4.1	0.0

TABLE 6. (Cont)

Time: 1214

Run Number 7718

t_{max} = 3.3μs

E_{total} = 204.5 J

R_p = 0.7μm

Q_α = 0.1469

Beam Lobe Number (from center)	P_{max} (W)	Time to Boil and Evaporate (μs)	Fraction of Energy in Remaining Portion of Pulse
0	2.32×10^7	1.73×10^{-1}	0.90
1	1.05×10^7	2.85×10^{-1}	0.84
2	7.81×10^6	3.89×10^{-1}	0.78
3	4.59×10^6	6.96×10^{-1}	0.62
4	1.86×10^6	2.44	0.65×10^{-1}
5	3.72×10^5	>3.3	0.0

Time: 1221

Run Number 7719

t_{max} = 3.0μs

E_{total} = 200 J

R_p = 0.6μm

Q_α = 0.1274

0	2.49×10^7	1.59×10^{-1}	0.90
1	1.13×10^7	2.61×10^{-1}	0.83
2	8.40×10^6	3.58×10^{-1}	0.78
3	4.93×10^6	6.42×10^{-1}	0.62
4	2.00×10^6	2.28	0.66×10^{-1}
5	4.00×10^5	>3.0	0.0

TABLE 6. (Cont)

Time: 1227

Run Number 7720

t_{max} = 3.3μs

E_{total} = 198 J

R_p = 0.45μm

Q_α = 0.0937

Beam Lobe Number (from center)	P_{max} (W)	Time to Boil and Evaporate (μs)	Fraction of Energy in Remaining Portion of Pulse
0	2.24×10^7	1.81×10^{-1}	0.89
1	1.02×10^7	2.96×10^{-1}	0.83
2	7.56×10^6	4.06×10^{-1}	0.77
3	4.44×10^6	7.30×10^{-1}	0.60
4	1.80×10^6	2.73	0.34×10^{-1}
5	3.60×10^5	>3.3	0.0

Time: 1232

Run Number 7721

t_{max} = 3.7μs

E_{total} = 193.2 J

R_p = 0.40μm

Q_α = 0.0828

0	1.95×10^7	2.09×10^{-1}	0.89
1	8.88×10^6	3.42×10^{-1}	0.82
2	6.58×10^6	4.70×10^{-1}	0.76
3	3.86×10^6	8.48×10^{-1}	0.59
4	1.37×10^6	3.53	0.34×10^{-2}
5	3.13×10^5	>4.0	0.0

CALCULATIONS, PART II: COLLECTIVE EFFECT

From these results one can calculate the net clearing effect on the beam. This punch-through phenomenon will be illustrated in the following calculations. For this purpose the particle size corresponding to the peak absorption for selected settling times will be used.

The expenditure of energy as a function of aerosol loading can be calculated from

$$E(L) = E(t = 0 \text{ to } t')e^{-\alpha x} + E(t = \text{to } t_{pulse})$$

$$\cong e^{-\alpha L} \int_0^{t'} P(t)dt + \int_{t'}^{t_{pulse}} P(t)dt ,$$

where t' is the time to evaporate and t_{pulse} is the total pulse duration. Here t' will have been increased over that of the single particle function as a result of the mass loading. For particles of given size and composition, t' is an inverse function of P_{max}. (L) represents the path length within the aerosol medium. The time to evaporate at a given position in the measurement is now dependent on that position although the above equation is written as though it depends only on the end point. This simplification does not significantly alter the results here. The smoke of phosphorus clears significantly for a fairly broad range of aerosol absorption coefficients (or alternatively a range of aerosol mass loading values). For relatively low absorption coefficients, clearing can do little to enhance the total energy transmitted. The enhancement due to clearing will be determined by the above presentation and, using this technique, can be extended to absorption coefficients of several tens per kilometer (typical field values) for even the relatively low energy system of these tests. Clearing continues to be significant for this (and other volatile) aerosols to, roughly, the loading at which beam energy is consumed in the evaporation process. Screening of available energy for particles farther from the source causes an increase in t' at about 25 km^{-1} (effectively) though the increase depends somewhat on factors such as particle size and relative humidity. For the calculations to follow, open air dispersal of WP was assumed; therefore, the peak absorption is for particles of 1μm to 1.2μm radius (see early-time data of figure 11). For all tests in the trench, particle radii became progressively smaller at similar rates; and the attenuation also decreased (on the average) throughout the test. The incorporatin of the bulk attenuation into the calculation of t' yields the results of figure 25. Table 5 shows that particle size and Lorenz-Mie efficiencies vary such as to hold t', the time to evaporate the particles, nearly constant (independent of particle size). Of course, particles with large radii require more energy to evaporate. The form of the curve, that is, curving over quickly at the top (on a semilog plot) augurs for the efficiency of the punch-through effect

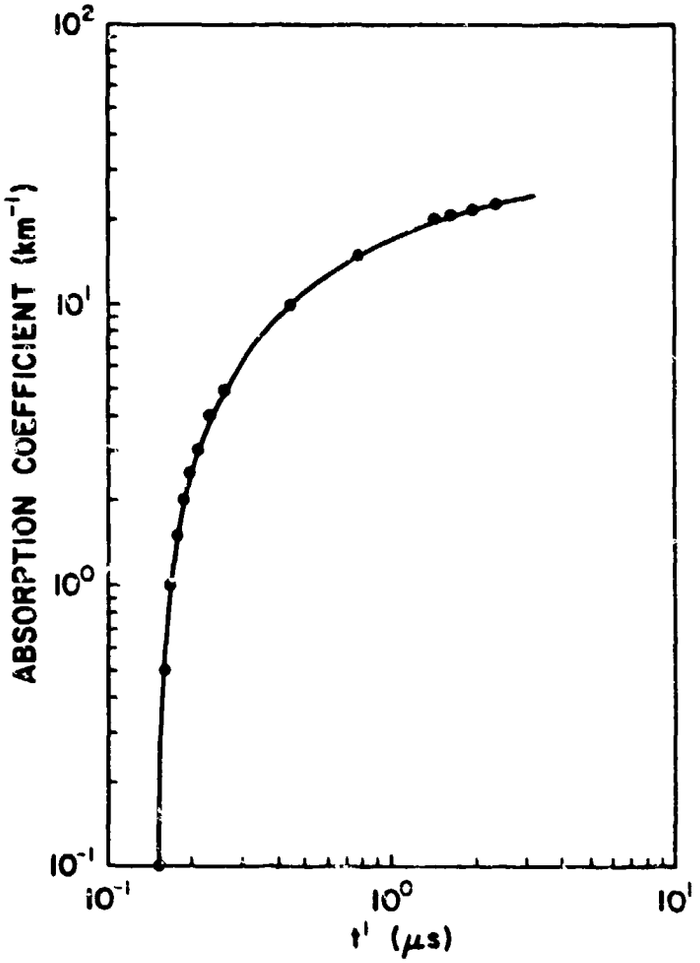

Figure 25. Time to evaporate center lobe in loaded aerosol medium. Loading given by absorption coefficient. E_{total} = 40.0 J (in lobe), R_p = 1μm, t_{pulse} = 3.2μs.

since it conveys that the time to evaporate increases rapidly with the absorption coefficient only for relatively high values of the coefficient. The remaining step is to show the relative improvement in the energy transmitted when punch-through occurs (table 7 and figure 26). The improvement in energy transmitted is truly significant--even though the pulsed laser on which the calculated parameters were based on a relatively small one.

Generally, thermal blooming and evaporative clearing effects are interactive; that is, the power density is affected by the thermal blooming which in turn affects the evaporative clearing. Thermal blooming depends on beam parameters (power density, pulse length, and pulse shape) and atmospheric parameters (gaseous and particulate absorption, crosswinds, and turbulence). Appendix F shows that blooming effects on the test beam are not expected to be strong; therefore, for this analysis, these effects have been ignored.

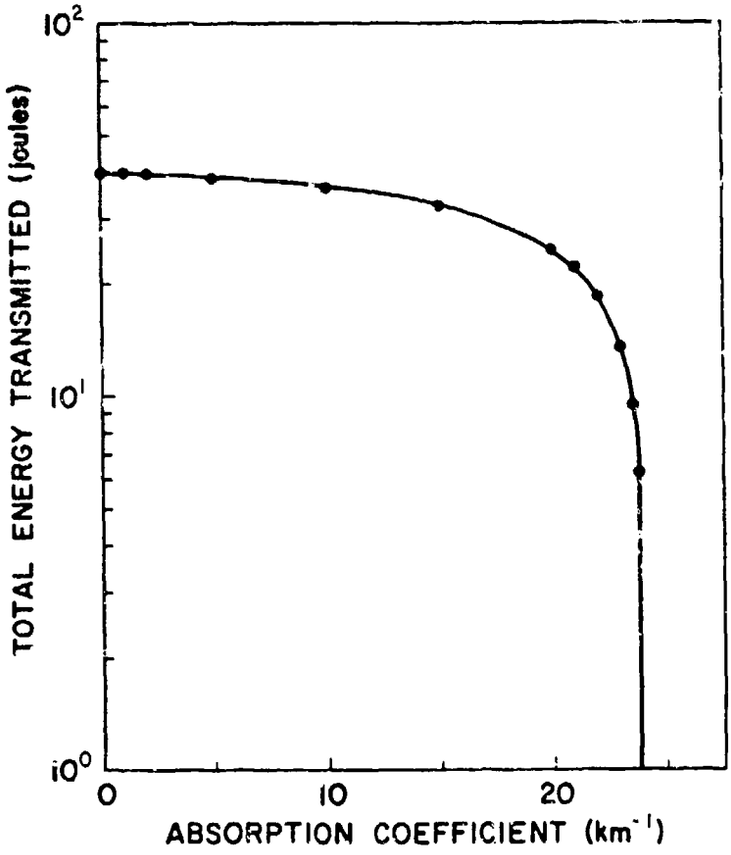

Figure 26. Total energy transmitted in center spot as a function of absorption coefficient for the WP-smoke aerosol. No gaseous absorption effects included.

CONCLUSIONS

Aerosol characterization performed on the smoke of WP was used to calculate punch-through or evaporative clearing on a pulsed CO_2 laser beam. This effect can be significant for HEL use. High energy pulsed CO_2 laser beams can effectively penetrate red phosphorus (RP), WP countermeasure smoke, though the degree of efficiency depends on beam and aerosol parameters. This effectiveness is related to the volatility and absorbing qualities of the smoke particles. Repetitive and/or long pulses can encounter strong thermal blooming due to the high level of aerosol absorption which counteracts the clearing effect. This report discusses the development of an analytical model and its application to aerosol parameters that derive from measurements in an extended enclosure at the MICOM in Huntsville, AL, and then to aerosol parameters that are more typical of atmospheric dispersion of the smoke (represented primarily by relatively large diameter particles). The laser beam parameters in both cases are relevant to a high energy research laser owned by MICOM and used for propagation studies in the above-mentioned enclosure during the in situ aerosol measurments presented in this report. Aerosol absorption measurements used in situ aerosol spectrophones developed at ASL. Thermal blooming (the stated original objective of the MICOM exploratory measurements program) is calculated in this report to be minimal for the beam parameters of the MICOM (S^3) laser as used in these tests and therefore is not expected to significantly affect the calculations of the clearing phenomenon.

TABLE 7. PARAMETERS SHOWING EFFICIENCY OF PUNCH-THROUGH FOR E_{TOTAL} = 40 J FOR CENTER LOBE.

(1)	(2)	(3)	(4)	(5)	(6)	(7)	(8)
α, Aerosol Absorption Coefficient (km^{-1})	$\alpha \times L$ ($L = 10^{-1}$km)	t' Time to Evaporate Aerosol	On-Target Energy Without Clearing, E/40 for $\alpha \times L$	$\frac{t_{pulse} - t'}{t_{pulse}}$	$\frac{t' \times 40}{t_{pulse}}$ (J)	(5) x 40 (J)	On-Target Energy With Clearing (6) + (7)/40
0.0	0.0	1.52×10^{-7}	1.00	0.953	1.9	38.1	1.00
0.1	0.001	1.54×10^{-7}	0.99	0.952	1.91	38.08	1.00
0.5	0.05	1.60×10^{-7}	0.95	0.950	1.9	38.00	1.00
1.0	0.10	1.68×10^{-7}	0.90	0.948	1.89	37.90	0.99
1.5	0.15	1.78×10^{-7}	0.86	0.944	1.91	37.80	0.99
2.0	0.20	1.87×10^{-7}	0.82	0.942	1.92	37.70	0.99
2.5	0.25	1.97×10^{-7}	0.78	0.938	1.92	37.50	0.98
3.0	0.30	2.08×10^{-7}	0.74	0.933	1.92	37.40	0.98
4.0	0.40	2.30×10^{-7}	0.67	0.930	1.93	37.20	0.98
5.0	0.50	2.56×10^{-7}	0.61	0.920	1.95	36.80	0.97
10.0	1.00	4.34×10^{-7}	0.37	0.864	2.01	34.60	0.92
15.0	1.50	7.56×10^{-7}	0.22	0.764	2.08	30.60	0.82
20.0	2.00	1.41×10^{-6}	0.14	0.559	2.47	22.40	0.62
21.0	2.10	1.63×10^{-6}	0.12	0.491	2.45	19.60	0.55
22.0	2.20	1.92×10^{-6}	0.11	0.400	2.64	16.00	0.47
23.0	2.30	2.34×10^{-6}	0.10	0.269	2.93	10.80	0.34
23.5	2.35	2.70×10^{-6}	0.095	0.156	3.21	6.24	0.24
23.7	2.37	2.97×10^{-6}	0.093	0.072	2.45	2.88	0.16
23.8	2.38	$>3.2 \times 10^{-6}$	0.093	----	----	----	----
24.0	2.40	$>3.2 \times 10^{-6}$	0.091	-----	----	----	----

REFERENCES

1. Gebhardt, F. G., 1976, "High power laser propagation," Appl Opt, 15(6):1479.

2. Bruce, C. W., and R. G. Pinnick, 1977, "In-situ measurements of aerosol absorption with a resonant CW laser spectrophone," Appl Opt, 16:1762.

3. Bruce, C. W., and Y. P. Yee, 1980, "In-situ measurement of the ratio of aerosol absorption to extinction coefficient," Appl Opt, 19:1893.

4. Kerr, E. L., and J. G. Attwood, 1968, "The laser illuminated absorptivity spectrophone: A method for measurement of weak absorptivity in gases at laser wavelengths," Appl Opt, 7:915.

5. Kreutzer, L. B., 1971, "Ultralow gas concentration infrared absorption spectroscopy," Appl Phys, 42:2934.

6. Yee, Y. P., C. W. Bruce, and R. J. Brewer, 1980, Gaseous/Particulate Absorption Studies at WSMR Using Laser Sourced Spectrophones, ASL-TR-0065, US Army Atmospheric Sciences Laboratory, White Sands Missile Range, NM.

7. Yin, P. K. L., and R. K. Long, 1968, "Atmospheric absorption at the line center of P(20) CO_2 laser radiation," Appl Opt, 7:1551.

8. Shumate, M. S., et al, 1976, "Water vapor absorption of carbon dioxide laser radiation," Appl Opt, 15:2480.

9. Hanel, G., and K. Bullrich, 1978, "Physico-chemical property models of tropospheric aerosol particles," Beitrage Zur Physik der Atmosphare, 51:129.

10. Querry, M. R., and I. L. Tyler, 1978, "Complex refractive indices in the infrared for H_3PO_4 in water," J Opt Soc Am, 68:1404.

11. Glicker, S. L., 1971, "Propagation of a 10.6μm laser through a cloud including droplet vaporization," Appl Opt, 10:644

12. Sutton, G. W., 1978, "Fog hole boring with pulsed high energy lasers: An exact solution including scattering and absorption," Appl Opt, 17:3424.

APPENDIX A

CONSTANTS USED IN THE CALCULATIONS OF NONLINEAR EFFECTS

$\bar{\rho}_m$ = 1.75 g/cc (bulk density)

c = 0.475 (cal/gm)/ C (specific heat capacity)

$\bar{H}$ = 266 cal/gm (latent heat of vaporization)

T = 323 K (ambient temperature)

T_{BP} = 443.7 K (boiling point temperature)

R_B = 0.91 cm center spot
0.778 cm side lobes (beam radius)

APPENDIX B

SAMPLE PULSE SHAPES

CO_2 Laser Pulse Width

0.5μs/div

0.1 V/div

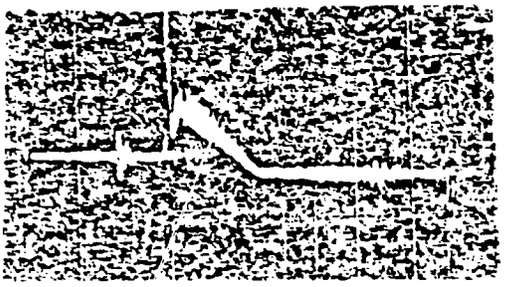

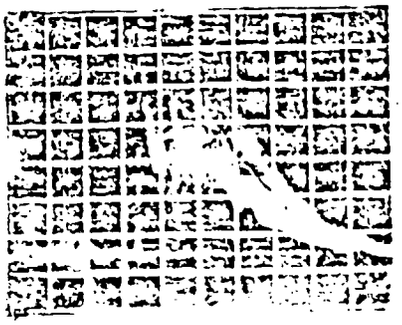

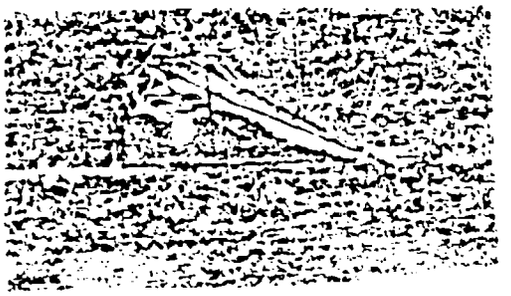

APPENDIX C

NEAR, NEAR FIELD BURN PATTERN

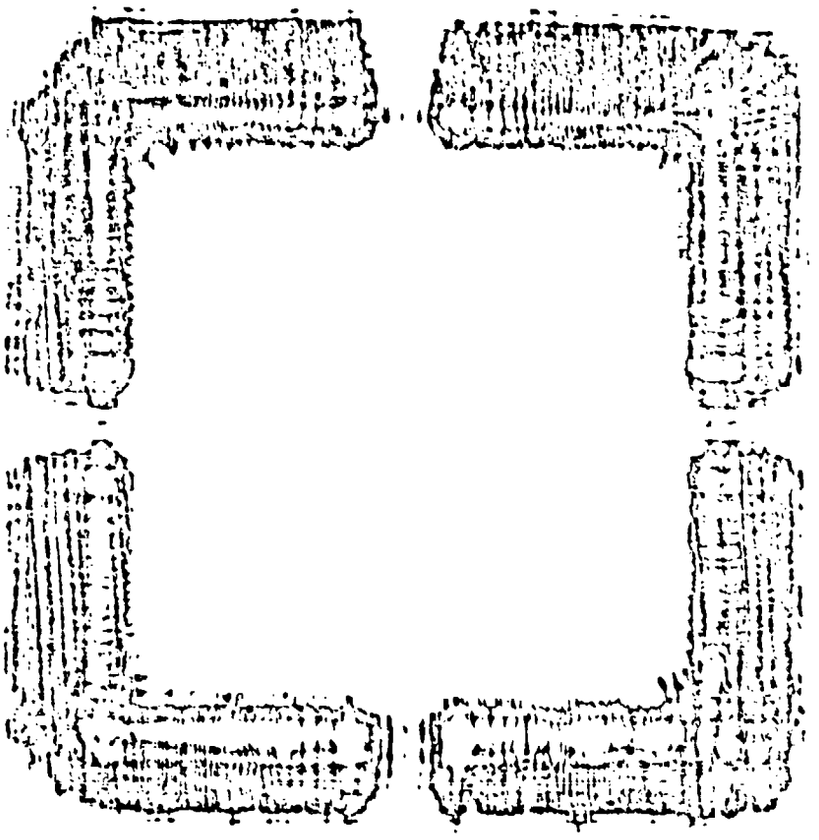

Run Number	Joules	Discharge Voltage
7715	0.825	39.5 kV
7716	0.900	36.0 kV
7717	1.500	35.9
7718	1.560	35.3
7719	1.512	35.9
7720	1.220	35.4
7721	1.320	35.4
7722	1.300	29.9 (prefire)

APPENDIX D

FAR FIELD PATTERN AT TARGET SITE FOR LASER CORRESPONDING TO NEAR FIELD BURN PATTERN OF APPENDIX C

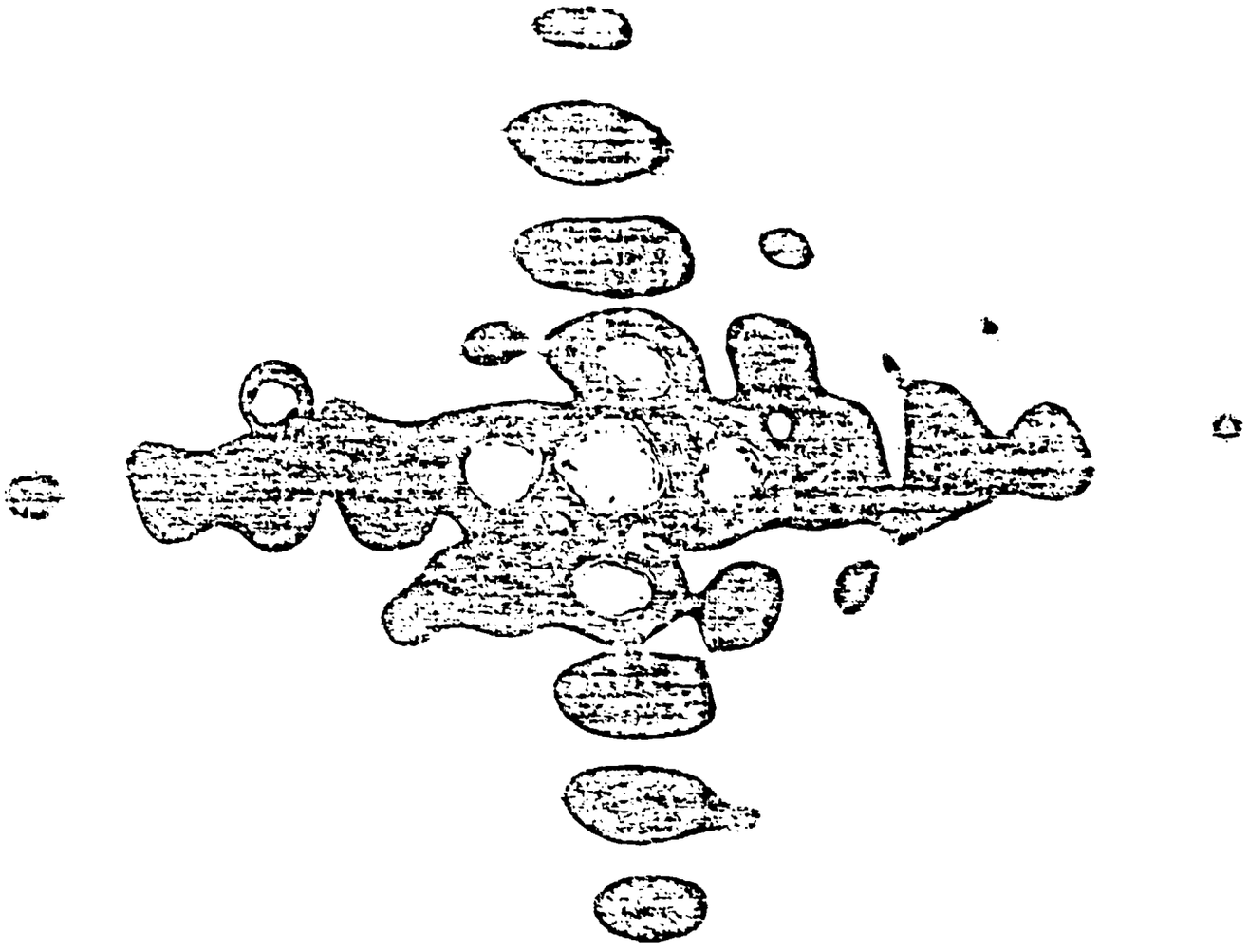

APPENDIX E

METHOD OF ESTIMATING ENERGY DISTRIBUTION IN THE BEAM FOR S^3 LASER BEAM

Data on hand consist of:

1. Burn pattern reproductions in actual size for field;
2. Near field burn pattern (not useful);
3. Some dimensions on laser,

   that is, a. Unstable resonator central reflector 7.57 cm "square";

   b. no outside limit (beam overfills square so beam energy cuts off at about 10 cm. This is not adequate. This outside limit must be calculated);

   c. beam take off and reflector supports are $\approx$ 0.3 inches wide;

   d. distance from laser to target is 136 m.

Thus, the output aperture geometry is as shown in figure E-1.

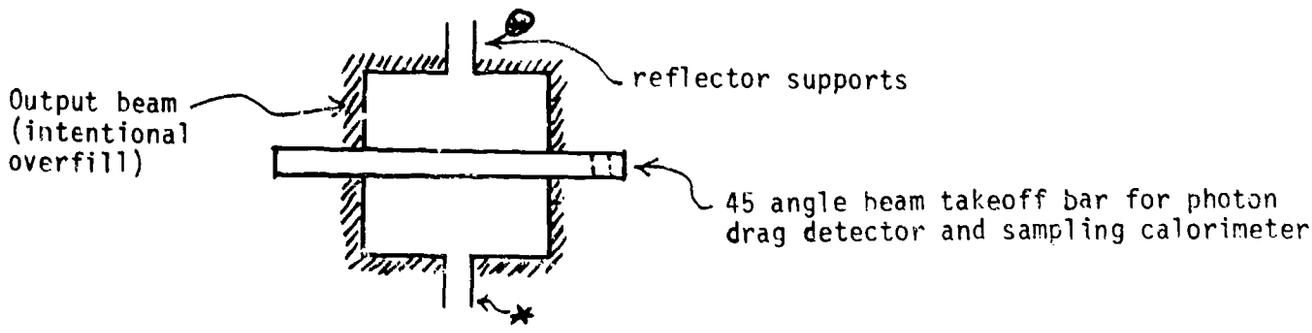

Figure E-1. S^3 laser output geometry.

Approximation: Use central arrays of orthogonal twin slit patterns, that is,

$$I = \frac{\sin^2\beta}{\beta^2} \left(\cos^2 \alpha\right) ,$$

$$\beta = \frac{\Pi}{\lambda} b \sin \theta ,$$

$$\alpha = \frac{\Pi}{\lambda} d \sin \theta ,$$

where b is the effective slit width at the output of the unstable resonator and d is the center-to-center distance of the output beam between the parallel sides.

First we calculate the viewing angle, θ, in terms of the displacement from the center of the arrays,

$$\sin \theta = \frac{x(\text{cm})}{1.36 \times 10^4} .$$

We use the far field burn pattern* and the double-slit part of the calculation to find the critical dimension, b.

$$\alpha = \frac{\Pi}{\lambda} d \sin \theta ,$$

where d = 7.56 cm + 1.0 x (gap width in centimeters).

The $\cos^2 \left(\frac{\Pi}{\lambda} d \frac{x}{1.36 \times 10^4}\right)$ factor gives the fine grain pattern under the single aperture intensity envelope. Maxima in the pattern are determined by

$$\frac{d[\cos(c'dx)]}{dx} = -c' \sin c'dx = 0 ,$$

*Appendix D

where

$$c' = \frac{\Pi}{\lambda} \frac{1}{1.36 \times 10^4} = 0.2179 \text{ cm}^{-1}$$

This condition is met when

$$c'dx = 0, \Pi, 2\Pi \ldots .$$

First, when $x = 0$;

second, when $x = \frac{\Pi}{c'd}$.

Then from the photo of the burn pattern (displacements, x, to five intensity lobes),

$$d = \langle 9.09 \text{ cm} \rangle \pm 0.07 \text{ cm (or } \pm 8 \text{ percent)} .$$

Calculating the quite critical parameter b for the diffraction envelope $\frac{\sin^2\beta}{\beta}$,

that is, 9.09 cm (twin slit center-to-center separation)

<u>7.56 cm</u> (twin slit inside dimension)

b = 1.53 cm (2 x (1/2) x slit width) .

Therefore,

$$\frac{\Pi}{\lambda} b = 4.535 \times 10^3 ;$$

$$\frac{\Pi}{\lambda} d = 2.694 \times 10^4 .$$

The calculations also need to be done for the maxima of the lobes. The average separation from the determination of d could be used,

$$x = \underbrace{0, \ 1.6}_{1.6}, \underbrace{\ 3.13}_{1.53}, \underbrace{\ 4.77}_{1.64}, \underbrace{\ 6.37}_{1.6} \text{ cm}$$

that is,

$$x = \langle 1.593 \rangle \pm 0.040 \text{ (or } \pm 2.5 \text{ percent)} .$$

From this,

$$\sin \theta = 1.171 \times 10^{-4} .$$

Now the relative intensities in the lobes of the far field pattern can be calculated (table E-1).

TABLE E-1. CALCULATION OF RELATIVE INTENSITIES FOR S^3 LASER BEAM LOBES

Can See?	Spot No.	Sin θ	Single Slit	Double Slit	$I_{relative}$
X	0(ctr)	0	2.00	1.00	2.0
X	1	1.171×10^{-4}	0.909	0.999	9.09×10^{-1}
X	2	2.342×10^{-4}	0.676	0.999	6.76×10^{-1}
X	3	3.513×10^{-4}	0.394	0.998	3.93×10^{-1}
X	4	4.684×10^{-4}	0.1604	0.997	1.60×10^{-1}
No	5	5.855×10^{-4}	0.0309	0.995	3.08×10^{-2}
No	6	7.026×10^{-4}	1.95×10^{-4}	0.994	1.95×10^{-4}

It will be assumed that all the energy is in the center and five wing spots in each direction (21 spots).

The intensity is then scaled for fraction of total power (10.675 norm).

	$I_{\hat{r}}$	$I_{\%}$
0(ctr)	1.87×10^{-1}	18.7
1	8.52×10^{-2}	8.5
2	6.33×10^{-2}	6.3
3	3.68×10^{-2}	3.7
4	1.50×10^{-2}	1.5
5	2.89×10^{-3}	0.3

The final step here is to obtain the lobe associated numbers giving the fractional power densities. To obtain these numbers divide the above values by 1.90 for all but the center lobe. For that lobe, divide by 2.60 cm^2. The result is in the text.

APPENDIX F

HIGH-ENERGY SINGLE-PULSE PROPAGATION ESTIMATES

High-energy laser (HEL) propagation is dependent upon a variety of atmospheric conditions and beam parameters. Some of the more important atmospheric factors involved are absorption, turbulence, and crosswinds. Thermal blooming and gas breakdown thresholds may be calculated from these factors.[1] In this appendix the occurrence of these two effects on a CO_2 HEL beam is formulated in terms of limitations on pulse length.[2] Assuming a fixed total pulse energy, if the actual pulse length of the laser beam is too short, then the problem of gas breakdown becomes important and is the dominant mechanism that restricts the energy fluence. On the other hand, if the pulse length is too long, the energy fluence on target drops significantly as a result of transient thermal blooming. These two effects deleterious to HEL propagation are thus minimal for a range of pulse lengths, t_p, between some minimum pulse length, t_m, due to gas breakdown and less than some "saturated" pulse length, t_s, due to transient thermal blooming effects; that is, $t_m < t_p < t_s$.

The saturation time, defined as the time at which the instantaneous peak irradiance at the target has dropped to about 10 percent of its initial value,[3] may be written as follows:

$$t_s = 0.08\left(\frac{n_o \rho_o c_p}{-n_t c_s^2 \alpha_{abs} f q_p}\right)^{1/2} \frac{\lambda^2 Z}{D E_p^{1/2}},$$

where

n_o = refractive index

ρ_o = density

c_p = specific heat at constant pressure

n_t = coefficient of index change with respect to temperature

c_s = acoustic wave velocity

---

[1] F. G. Gebhardt, 1976, "High power laser propagation," Appl Opt, 15:1479

[2] S. L. Glicker, 1971, "Propagation of a 10.6μm laser through a cloud including droplet vaporization," Appl Opt, 10:644

[3] P. B. Ulrich, 1973, "Requirements for experimental verification of thermal-blooming computer results," J Opt Soc Am, 63:897

α_{abs} = absorption coefficient

f = correction factor that accounts for finite attenuation and is a function of $\alpha_t Z$, the optical depth;

that is,

$$f = \frac{2}{(\alpha_t Z)^2} \left[\alpha_t Z - 1 + e^{-\alpha_t Z} \right]$$

α_t = total extinction coefficient

q_p = correction factor that accounts for varying degrees of focusing;

that is,

$$f = \frac{X^4 - 1 - 4 \ln X}{8X^2 (X - 1)^2} \quad \text{where } X = \frac{A_o}{A_d}$$

A_o = 1/e beam radius

A_d = vacuum 1/e beam radius at the range Z for an infinite Gaussian source including diffraction effects and poor beam quality,

that is

$$A_1^2 = \frac{\beta^2 Z^2}{k^2 A_o^2} + \left(A_o^2 \quad 1 - \frac{Z}{F} \right)^2$$

where the β parameter characterizes the beam quality of the source in terms of its far-field or focused beam radius.

$k = \frac{2\Pi}{\lambda}$

λ = wavelength of the source

Z = range

R = focal range of the beam

$D = 2\sqrt{2}\, A_o$ = aperture diameter

E_p = total pulse energy

The minimum pulse length limit, t_m, on the maximum peak target irradiance as imposed by the gas breakdown threshold is simplified as follows:

$$t_m = 1.6 \frac{D^2 E_p}{\lambda^2 Z^2 I_{BD}} e^{-\alpha_t Z} ,$$

where I_{BD} is the gas breakdown threshold for the atmosphere depending upon many factors such as dust aerosol density, laser wavelength, pulse length, and focal spot size as discussed by Morgan.[4] For our calculations we assumed typical values for the atmosphere of $n_o = 1$, $\rho_o = 1\ kg/m^3$, $c_p = 10^3$ J/kg - K, $-n_t = 10^{-6} K^{-1}$, $c_s = 340$ m/s, and $I_{BD} = 10^7 W/cm^2$, which is appropriate for $\lambda = 10.6\mu m$.

The following table is a compilation of t_s values for various absorption coefficients as the density of the WP cloud decreases with time after initial dispersion.

---

[4]C. G. Morgan, 1975, "Laser-induced breakdown of gases," Rep Prog Phys, 38:621

Center lobe (0)
Energy = 40.0 J
Effective beam diameter aperture = 2.57 cm

$\alpha_{abs}(km^{-1})$	f	q	$t_s(s)$
50	0.321	3.81	3.23×10^{-6}
25	0.506	3.81	3.75×10^{-6}
10	0.736	3.81	4.92×10^{-6}
5	0.852	3.81	6.46×10^{-6}
2.5	0.922	3.81	8.79×10^{-6}
1.0	0.967	3.81	13.6×10^{-6}

First side lobe (1)
Energy = 18.1 J
Effective beam diameter aperture = 2.20 cm

$\alpha_{abs}(km^{-1})$	f	q	$t_s(s)$
50	0.321	7.36	4.16×10^{-6}
25	0.506	7.36	4.69×10^{-6}
10	0.736	7.36	6.14×10^{-6}
5	0.852	7.36	8.08×10^{-6}
2.5	0.922	7.36	10.9×10^{-6}
1.0	0.967	7.36	16.9×10^{-6}

Second side lobe (2)
Energy = 13.5 J
Effective beam diameter aperture = 2.20 cm

$\alpha_{abs}(km^{-1})$	f	q	$t_s(s)$
50	0.321	7.36	4.82×10^{-6}
25	0.506	7.36	5.43×10^{-6}
10	0.736	7.36	7.11×10^{-6}
5	0.852	7.36	9.35×10^{-6}
2.5	0.922	7.36	12.7×10^{-6}
1.0	0.967	7.36	19.6×10^{-6}

Third side lobe (3)
Energy = 7.88 J
Effective beam diameter aperture = 2.20 cm

$\alpha_{abs}(km^{-1})$	f	q	$t_s(s)$
50	0.321	7.36	6.31×10^{-6}
25	0.506	7.36	7.10×10^{-6}
10	0.736	7.36	9.31×10^{-6}
5	0.852	7.36	12.2×10^{-6}
2.5	0.922	7.36	16.6×10^{-6}
1.0	0.967	7.36	25.7×10^{-6}

Fourth side lobe (4)
Energy = 3.2 J
Effective beam diameter aperture = 2.20 cm

$\alpha_{abs}(km^{-1})$	f	q	$t_s(s)$
50	0.321	7.36	9.89×10^{-6}
25	0.506	7.36	11.1×10^{-6}
10	0.736	7.36	14.6×10^{-6}
5	0.852	7.36	19.2×10^{-6}
2.5	0.922	7.36	26.1×10^{-6}
1.0	0.967	7.36	40.3×10^{-6}

The following table is a compilation of typical t_m values for various absorption coefficients as the density of the WP smoke cloud decreases with time after initial dispersion

D (m)	E_p (J)	I_{BD} (W/cm^2)	α_t (km^{-1})	$t_m(s)$
2.57×10^{-7}	80	10^7	50	5.07×10^{-9}
2.56×10^{-7}	80	10^7	25	6.17×10^{-8}
2.57×10^{-7}	80	10^7	10	2.77×10^{-7}
2.57×10^{-7}	80	10^7	5	4.56×10^{-7}
2.57×10^{-7}	80	10^7	2.5	5.85×10^{-7}
2.57×10^{-7}	80	10^7	1.0	6.81×10^{-7}

Matching the average pulse length t_p of the S^3 high energy CO_2 laser output to the minimum pulse length t_m requirement and to the upper limit on the saturation thermal blooming pulse length t_s, we find that t_p is well above the gas breakdown threshold for a variety of total extinction coefficients α_t. Also for absorption coefficients less than 50 km^{-1}, t_p is below the saturated pulse length t_s. For example, at the center lobe (0) with high α_{abs} and $\alpha_t \sim$ 50 km^{-1}, $t_p \sim 3.2\mu s$ meets the requirements to maximize the single pulse fluence delivery since $0.005\mu s < t_p < 3.33\mu s$. At relatively low total extinction values $\alpha_t \sim 1.0$ km^{-1}, t_p is again well within the pulse length limitations imposed, that is, $0.58\mu s < t_p < 13.6\mu s$ in the center lobe (0). Thus we see that thermal blooming and gas breakdown effects are not significant factors in punch-through clearing as formulated in this article for the S^3 CO_2 HEL.

DISTRIBUTION LIST

Commander
US Army Aviation Center
ATTN: ATZQ-D-MA
Fort Rucker, AL 36362

Chief, Atmospheric Sciences Div
Code ES-81
NASA
Marshall Space Flight Center, AL 35812

Commander
US Army Missile Command
ATTN: DRDMI-RRA/Dr.O. M. Essenwanger
Redstone Arsenal, AL 35809

Commander
US Army Missile Command
ATTN: DRSMI-OG (B. W. Fowler)
Redstone Arsenal, AL 35809

Commander
US Army Missile R&D Command
ATTN: DRDMI-TEM (R. Haraway)
Redstone Arsenal, AL 35809

Redstone Scientific Information Center
ATTN: DRSMI-RPRD (Documents)
US Army Missile Command
Redstone Arsenal, AL 35809

Commander
HQ, Fort Huachuca
ATTN: Tech Ref Div
Fort Huachuca, AZ 85613

Commander
US Army Intelligence
Center & School
ATTN: ATSI-CD-MD
Fort Huachuca, AZ 85613

Commander
US Army Yuma Proving Ground
ATTN: Technical Library
Bldg 2105
Yuma, AZ 85364

Dr. Frank D. Eaton
Geophysical Institute
University of Alaska
Fairbanks, AK 99701

Naval Weapons Center
Code 3918
ATTN: Dr. A. Shlanta
China Lake, CA 93555

Commanding Officer
Naval Envir Prediction Rsch Facility
ATTN; Library
Monterey, CA 93940

Sylvania Elec Sys Western Div
ATTN: Technical Reports Lib
PO Box 205
Mountain View, CA 94040

Geophysics Officer
PMTC Code 3250
Pacific Missile Test Center
Point Mugu, CA 93042

Commander
Naval Ocean Systems Center
(Code 4473)
ATTN: Technical Library
San Diego, CA 92152

Meteorologist in Charge
Kwajalein Missile Range
PO Box 67
APO San Francisco, CA 96555

Director
NOAA/ERL/APCL R31
RB3-Room 567
Boulder, CO 80302

Dr.B. A. Silverman D-1200
Office of Atmos Resources Management
Water and Power Resources Service
PO Box 25007Denver Federal Center, Bldg. 67
Denver, CO 80225

Hugh W. Albers (Executive Secretary)
CAO Subcommittee on Atmos Rsch
National Science Foundation Room 510
Washington, DC 2055

Dr. Eugene W. Bierly
Director, Division of Atmos Sciences
National Scinece Foundation
1800 G Street, N.W.
Washington, DC 20550

Commanding Officer
Naval Research Laboratory
Code 2627
Washington, DC 20375

Defense Communications Agency
Technical Library Center
Code 222
Washington, DC 20305

Director
Naval Research Laboratory
Code 5530
Washington, DC 20375

Dr. J. M. MacCallum
Naval Research Laboratory
Code 1409
Washington, DC 20375

HQDA (DAEN-RDM/Dr. de Percin)
Washington, DC 20314

The Library of Congress
ATTN: Exchange & Gift Div
Washington, DC 20540
2

Mil Asst for Atmos Sci Ofc of
the Undersecretary of Defense
for Rsch & Engr/E&LS - RM 3D129
The Pentagon
Washington, DC 20301

AFATL/DLODL
Technical Library
Eglin AFB, FL 32542

Naval Training Equipment Center
ATTN: Technical Information Center
Orlando, FL 32813

Technical Library
Chemical Systems Laboratory
Aberdeen Proving Ground, MD 21010

US Army Materiel Systems
Analysis Activity
ATTN: DRXSY-MP
APG, MD 21005

Commander
ERADCOM
ATTN: DRDEL-PA/ILS/-ED
2800 Powder Mill Road
Adelphi, MD 20783

Commander
ERADCOM
ATTN: DRDEL-ST-T (Dr. B. Zarwyn)
2800 Powder Mill Road
Adelphi, MD 20783
02

Commander
Harry Diamond Laboratories
ATTN: DELHD-CO
2800 Powder Mill Road
Adelphi, MD 20783

Chief
Intel Mat Dev & Spt Ofc
ATTN: DELEW-WL-I
Bldg 4554
Fort George G. Mead, MD 20755

Acquisitions Section, IRDB-D823
Library & Info Svc Div, NOAA
6009 Executive Blvd.
Rockville, MD 20752

Naval Surface Weapons Center
White Oak Library
Silver Spring, MD 20910

Air Force Geophysics Laboratory
ATTN: LCC (A. S. Carten, Jr.)
Hanscom AFB, MA 01731

Air Force Geophysics Laboratory
ATTN: LYD
Hanscom AFB, MA 01731

Meteorology Division
AFGL/LY
Hanscom AFB, MA 01731

The Environmental Research
Institute of MI
ATTN: IRIA Library
PO Box 8618
Ann Arbor, MI 48107

Mr. William A. Main
USDA Forest Service
1407 S. Harrison Road
East Lansing, MI 48823

Dr. A. D. Belmont
Research Division
PO Box 1249
Control Data Corp
Minneapolis, MN 55440

Commander
Naval Oceanography Command
Bay St. Louis, MS 39529

Commanding Officer
US Army Armament R&D Command
ATTN; DRDAR-TSS Bldg 59
Dover, NJ 07801

Commander
ERADCOM Scientific Advisor
ATTN: DRDEL-SA
Fort Monmouth, NJ 07703

Commander
ERADCOM Tech Support Activity
ATTN: DELSD-L
Fort Monmouth, NJ 07703

Commander
HQ, US Army Avionics R&D Actv
ATTN: DAVAA-O
Fort Monmouth, NJ 07703

Commander
USA Elect Warfare Lab
ATTN: DELEW-DA (File Cy)
Fort Monmouth, NJ 07703

Commander
US Army Electronics R&D Command
ATTN: DELCS-S
Fort Monmouth, NJ 07703

Commander
US Army Satellite Comm Agency
ATTN: DRCPM-SC-3
Fort Monmouth, NJ 07703

Commander/Director
US Army Combat Survl & Target
Acquisition Laboratory
ATTN. DELCS-D
Fort Monmouth, NJ 07703

Director
Night Vision & Electro-Optics Laboratory
ATTN: DELNV-L (Dr. R. Buser)
Fort Belvoir, VA 22060

Project Manager, FIREFINDER
ATTN: DRCPM-FF
Fort Monmouth, NJ 07703

PM, Firefinder/REMBASS
ATTN: DRCPM-FFR-TM
Fort Monmouth, NJ 07703

6585 TG/WE
Holloman AFB, NM 88330

AFWL/Technical Library (SUL)
Kirtland AFB, NM 87117

AFWL/WE
Kirtland, AFB, NM 87117

TRASANA
ATTN: ATAA-SL (D. Anguiano)
WSMR, NM 88002

Commander
US Army White Sands Missile Range
ATTN: STEWS-PT-AL
White Sands Missile Range, NM 88002

Rome Air Development Center
ATTN: Documents Library
TSLD (Bette Smith)
Griffiss AFB, NY 13441

Environmental Protection Agency
Meteorology Laboratory, MD 80
Rsch Triangle Park, NC 27711

US Army Research Office
ATTN: DRXRO-PP
PO Box 12211
Rsch Triangle Park, NC 27709

Commandant
US Army Field Artillery School
ATTN: ATSF-CD-MS (Mr. Farmer)
Fort Sill, OK 73503

Commandant
US Army Field Artillery School
ATTN: ATSF-CF-F
Fort Sill, OK 73503

Commandant
US Army Field Artillery School
ATTN: Morris Swett Library
Fort Sill, OK 73503

Commander
US Army Dugway Proving Ground
ATTN: STEDP-MT-DA-M
(Mr. Paul Carlson)
Dugway, UT 84022

Commander
US Army Dugway Proving Ground
ATTN: MT-DA-L
Dugway, UT 84022

US Army Dugway Proving Ground
ATTN: STEDP-MT-DA-T
(Dr. W. A. Peterson)
Dugway, UT 84022

Inge Dirmhirn, Professor
Utah State University, UMC 48
Logan, UT 84322

Defense Technical Information Center
ATTN: DTIC-DDA-2
Cameron Station, Bldg. 5
Alexandria, VA 22314
12

Commanding Officer
US Army Foreign Sci & Tech Cen
ATTN: DRXST-IS1
220 7th Street, NE
Charlottesville, VA 22901

Naval Surface Weapons Center
Code G65
Dahlgren, VA 22448

Commander
US Army Night Vision
& Electro-Optics Lab
ATTN: DELNV-D
Fort Belvoir, VA 22060

Commander
USATRADOC
ATTN: ATCD-FA
Fort Monroe, VA 23651

Commander
USATRADOC
ATTN: ATCD-IR
Fort Monroe, VA 23651

Dept of the Air Force
5WW/DN
Langley AFB, VA 23665

US Army Nuclear & Cml Agency
ATTN: MONA-WE
Springfield, VA 22150

Director
US Army Signals Warfare Lab
ATTN: DELSW-OS (Dr. Burkhardt)
Vint Hill Farms Station
Warrenton, VA 22186

Commander
US Army Cold Regions Test Cen
ATTN: STECR-OP-PM
APO Seattle, WA 98733

ATMOSPHERIC SCIENCES RESEARCH PAPERS

1. Lindberg, J.D., "An Improvement to a Method for Measuring the Absorption Coefficient of Atmospheric Dust and other Strongly Absorbing Powders," ECOM-5565, July 1975.
2. Avara, Elton, P., "Mesoscale Wind Shears Derived from Thermal Winds," ECOM-5566, July 1975.
3. Gomez, Richard B., and Joseph H. Pierluissi, "Incomplete Gamma Function Approximation for King's Strong-Line Transmittance Model," ECOM-5567, July 1975.
4. Blanco, A.J., and B.F. Engebos, "Ballistic Wind Weighting Functions for Tank Projectiles," ECOM-5568, August 1975.
5. Taylor, Fredrick J., Jack Smith, and Thomas H. Pries, "Crosswind Measurements through Pattern Recognition Techniques," ECOM-5569, July 1975.
6. Walters, D.L., "Crosswind Weighting Functions for Direct-Fire Projectiles," ECOM-5570, August 1975.
7. Duncan, Louis D., "An Improved Algorithm for the Iterated Minimal Information Solution for Remote Sounding of Temperature," ECOM-5571, August 1975.
8. Robbiani, Raymond L., "Tactical Field Demonstration of Mobile Weather Radar Set AN/TPS-41 at Fort Rucker, Alabama," ECOM-5572, August 1975.
9. Miers, B., G. Blackman, D. Langer, and N. Lorimier, "Analysis of SMS/GOES Film Data," ECOM-5573, September 1975.
10. Manquero, Carlos, Louis Duncan, and Rufus Bruce, "An Indication from Satellite Measurements of Atmospheric CO2 Variability," ECOM-5574, September 1975.
11. Petracca, Carmine, and James D. Lindberg, "Installation and Operation of an Atmospheric Particulate Collector," ECOM-5575, September 1975.
12. Avara, Elton P., and George Alexander, "Empirical Investigation of Three Iterative Methods for Inverting the Radiative Transfer Equation," ECOM-5576, October 1975.
13. Alexander, George D., "A Digital Data Acquisition Interface for the SMS Direct Readout Ground Station — Concept and Preliminary Design," ECOM-5577, October 1975.
14. Cantor, Israel, "Enhancement of Point Source Thermal Radiation Under Clouds in a Nonattenuating Medium," ECOM-5578, October 1975.
15. Norton, Colburn, and Glenn Hoidale, "The Diurnal Variation of Mixing Height by Month over White Sands Missile Range, N.M," ECOM-5579, November 1975.
16. Avara, Elton P., "On the Spectrum Analysis of Binary Data," ECOM-5580, November 1975.
17. Taylor, Fredrick J., Thomas H. Pries, and Chao-Huan Huang, "Optimal Wind Velocity Estimation," ECOM-5581, December 1975.
18. Avara, Elton P., "Some Effects of Autocorrelated and Cross-Correlated Noise on the Analysis of Variance," ECOM-5582, December 1975.
19. Gillespie, Patti S., R.L. Armstrong, and Kenneth O. White, "The Spectral Characteristics and Atmospheric CO2 Absorption of the Ho^{+3}:YLF Laser at 2.05μm," ECOM-5583, December 1975.
20. Novlan, David J. "An Empirical Method of Forecasting Thunderstorms for the White Sands Missile Range," ECOM-5584, February 1976.
21. Avara, Elton P., "Randomization Effects in Hypothesis Testing with Autocorrelated Noise," ECOM-5585, February 1976.
22. Watkins, Wendell R., "Improvements in Long Path Absorption Cell Measurement," ECOM-5586, March 1976.
23. Thomas, Joe, George D. Alexander, and Marvin Dubbin, "SATTEL — An Army Dedicated Meteorological Telemetry System," ECOM-5587, March 1976.
24. Kennedy, Bruce W., and Delbert Bynum, "Army User Test Program for the RDT&E-XM-75 Meteorological Rocket," ECOM-5588, April 1976.

25. Barnett, Kenneth M., "A Description of the Artillery Meteorological Comparisons at White Sands Missile Range, October 1974 – December 1974 (PASS) – Prototype Artillery [Meteorological] Sensor System," ECOM-5589, April 1976.
26. Miller, Walter B., "Preliminary Analysis of Data of Shot From Project 'PASS'," ECOM-5590, April 1976.
27. Avara, Elton P., "Error Analysis of Minimum Information and Smith's Direct Methods for Inverting the Radiative Transfer Equation," ECOM-5591, April 1976.
28. Yee, Young P., James D. Horn, and George Alexander, "Synoptic Thermal Wind Calculations from Radiosonde Observations Over the Southwestern United States," ECOM-5592, May 1976.
29. Duncan, Louis D., and Mary Ann Seagraves, "Applications of Empirical Corrections to NOAA-4 VTPR Observations," ECOM-5593, May 1976.
30. Miers, Bruce T., and Steve Weaver, "Applications of Meterological Satellite Data to Weather Sensitive Army Operations," ECOM-5594, May 1976.
31. Sharenow, Moses, "Redesign and Improvement of Balloon ML-566," ECOM-5595, June, 1976.
32. Hansen, Frank V., "The Depth of the Surface Boundary Layer," ECOM-5596, June 1976.
33. Pinnick, R.G., and E.B. Stenmark, "Response Calculations for a Commercial Light-Scattering Aerosol Counter," ECOM-5597, July 1976.
34. Mason, J., and G.B. Houdale, "Visibility as an Estimator of Infrared Transmittance," ECOM-5598, July 1976.
35. Bruce, Rufus E., Louis D. Duncan, and Joseph H. Pierluissi, "Experimental Study of the Relationship Between Radiosonde Temperatures and Radiometric-Area Temperatures," ECOM-5599, August 1976.
36. Duncan, Louis D., "Stratospheric Wind Shear Computed from Satellite Thermal Sounder Measurements," ECOM-5800, September 1976.
37. Taylor, F., P. Mohan, P. Joseph and T. Pries, "An All Digital Automated Wind Measurement System," ECOM-5801, September 1976.
38. Bruce, Charles, "Development of Spectrophones for CW and Pulsed Radiation Sources," ECOM-5802, September 1976.
39. Duncan, Louis D., and Mary Ann Seagraves, "Another Method for Estimating Clear Column Radiances," ECOM-5803, October 1976.
40. Blanco, Abel J., and Larry E. Taylor, "Artillery Meteorological Analysis of Project Pass," ECOM-5804, October 1976.
41. Miller, Walter, and Bernard Engebos, "A Mathematical Structure for Refinement of Sound Ranging Estimates," ECOM-5805, November, 1976.
42. Gillespie, James B., and James D. Lindberg, "A Method to Obtain Diffuse Reflectance Measurements from 1.0 to 3.0 μm Using a Cary 17I Spectrophotometer," ECOM-5806, November 1976.
43. Rubio, Roberto, and Robert O. Olsen, "A Study of the Effects of Temperature Variations on Radio Wave Absorption," ECOM-5807, November 1976.
44. Ballard, Harold N., "Temperature Measurements in the Stratosphere from Balloon-Borne Instrument Platforms, 1968-1975," ECOM-5808, December 1976.
45. Monahan, H.H., "An Approach to the Short-Range Prediction of Early Morning Radiation Fog," ECOM-5809, January 1977.
46. Engebos, Bernard Francis, "Introduction to Multiple State Multiple Action Decision Theory and Its Relation to Mixing Structures," ECOM-5810, January 1977.
47. Low, Richard D.H., "Effects of Cloud Particles on Remote Sensing from Space in the 10-Micrometer Infrared Region," ECOM-5811, January 1977.
48. Bonner, Robert S., and R. Newton, "Application of the AN/GVS-5 Laser Rangefinder to Cloud Base Height Measurements," ECOM-5812, February 1977.
49. Rubio, Roberto, "Lidar Detection of Subvisible Reentry Vehicle Erosive Atmospheric Material," ECOM-5813, March 1977.
50. Low, Richard D.H., and J.D. Horn, "Mesoscale Determination of Cloud-Top Height: Problems and Solutions," ECOM-5814, March 1977.

51. Duncan, Louis D., and Mary Ann Seagraves, "Evaluation of the NOAA-4 VTPR Thermal Winds for Nuclear Fallout Predictions," ECOM-5815, March 1977.
52. Randhawa, Jagir S., M. Izquierdo Carlos McDonald and Zvi Salpeter, "Stratospheric Ozone Density as Measured by a Chemiluminescent Sensor During the Stratcom VI-A Flight," ECOM-5816, April 1977.
53. Rubio, Roberto, and Mike Izquierdo, "Measurements of Net Atmospheric Irradiance in the 0.7- to 2.8-Micrometer Infrared Region," ECOM-5817, May 1977.
54. Ballard, Harold N., Jose M. Serna, and Frank P. Hudson Consultant for Chemical Kinetics, "Calculation of Selected Atmospheric Composition Parameters for the Mid-Latitude, September Stratosphere," ECOM-5818, May 1977.
55. Mitchell, J.E., R.S. Sagar, and R.O. Olsen, "Positive Ions in the Middle Atmosphere During Sunrise Conditions," ECOM-5819, May 1977.
56. White, Kenneth O., Wendell R. Watkins, Stuart A. Schleusener, and Ronald L. Johnson, "Solid-State Laser Wavelength Identification Using a Reference Absorber," ECOM-5820, June 1977.
57. Watkins, Wendell R., and Richard G. Dixon, "Automation of Long-Path Absorption Cell Measurements," ECOM-5821, June 1977.
58. Taylor, S.E., J.M. Davis, and J.B. Mason, "Analysis of Observed Soil Skin Moisture Effects on Reflectance," ECOM-5822, June 1977.
59. Duncan, Louis D. and Mary Ann Seagraves, "Fallout Predictions Computed from Satellite Derived Winds," ECOM-5823, June 1977.
60. Snider, D.E., D.G. Murcray, F.H. Murcray, and W.J. Williams, "Investigation of High-Altitude Enhanced Infrared Backround Emissions" (U), SECRET, ECOM-5824, June 1977.
61. Dubbin, Marvin H. and Dennis Hall, "Synchronous Meteorlogical Satellite Direct Readout Ground System Digital Video Electronics," ECOM-5825, June 1977.
62. Miller, W., and B. Engebos, "A Preliminary Analysis of Two Sound Ranging Algorithms," ECOM-5826, July 1977.
63. Kennedy, Bruce W., and James K. Luers, "Ballistic Sphere Techniques for Measuring Atomspheric Parameters," ECOM-5827, July 1977
64. Duncan, Louis D., "Zenith Angle Variation of Satellite Thermal Sounder Measurements," ECOM-5828, August 1977.
65. Hansen, Frank V., "The Critical Richardson Number," ECOM-5829, September 1977.
66. Ballard, Harold N., and Frank P. Hudson (Compilers), "Stratospheric Composition Balloon-Borne Experiment," ECOM-5830, October 1977.
67. Barr William C., and Arnold C. Peterson, "Wind Measuring Accuracy Test of Meteorological Systems," ECOM-5831, November 1977.
68. Ethridge, G.A. and F.V. Hansen, "Atmospheric Diffusion: Similarity Theory and Empirical Derivations for Use in Boundary Layer Diffusion Problems," ECOM-5832, November 1977.
69. Low, Richard D.H., "The Internal Cloud Radiation Field and a Technique for Determining Cloud Blackness," ECOM-5833, December 1977.
70. Watkins, Wendell R., Kenneth O. White, Charles W. Bruce, Donald L. Walters, and James D. Lindberg, "Measurements Required for Prediction of High Energy Laser Transmission," ECOM-5834, December 1977.
71. Rubio, Robert, "Investigation of Abrupt Decreases in Atmospherically Backscattered Laser Energy," ECOM-5835, December 1977.
72. Monahan, H.H. and R.M. Cionco, "An Interpretative Review of Existing Capabilities for Measuring and Forecasting Selected Weather Variables (Emphasizing Remote Means)," ASL-TR-0001, January 1978.
73. Heaps, Melvin G., "The 1979 Solar Eclipse and Validation of D Region Models," ASL-TR-0002, March 1978.

74. Jennings, S.G., and J.B. Gillespie, "M.I.E. Theory Sensitivity Studies - The Effects of Aerosol Complex Refractive Index and Size Distribution Variations on Extinction and Absorption Coefficients Part II: Analysis of the Computational Results," ASL-TR-0003, March 1978.

75. White, Kenneth O. et al, "Water Vapor Continuum Absorption in the 3.5μm to 4.0μm Region," ASL-TR-0004, March 1978.

76. Olsen, Robert O., and Bruce W. Kennedy, "ABRES Pretest Atmospheric Measurements," ASL-TR-0005, April 1978.

77. Ballard, Harold N., Jose M. Serna, and Frank P. Hudson, "Calculation of Atmospheric Composition in the High Latitude September Stratosphere," ASL-TR-0006, May 1978.

78. Watkins, Wendell R. et al, "Water Vapor Absorption Coefficients at HF Laser Wavelengths," ASL-TR-0007, May 1978.

79. Hansen, Frank V., "The Growth and Prediction of Nocturnal Inversions," ASL-TR-0008, May 1978.

80. Samuel, Christine, Charles Bruce, and Ralph Brewer, "Spectrophone Analysis of Gas Samples Obtained at Field Site," ASL-TR-0009, June 1978.

81. Pinnick, R.G. et al., "Vertical Structure in Atmospheric Fog and Haze and its Effects on IR Extinction," ASL-TR-0010, July 1978.

82. Low, Richard D.H., Louis D. Duncan, and Richard B. Gomez, "The Microphysical Basis of Fog Optical Characterization," ASL-TR-0011, August 1978.

83. Heaps, Melvin G., "The Effect of a Solar Proton Event on the Minor Neutral Constituents of the Summer Polar Mesosphere," ASL-TR-0012, August 1978.

84. Mason, James B., "Light Attenuation in Falling Snow," ASL-TR-0013, August 1978.

85. Blanco, Abel J., "Long-Range Artillery Sound Ranging: "PASS" Meteorological Application," ASL-TR-0014, September 1978.

86. Heaps, M.G., and F.E. Niles, "Modeling the Ion Chemistry of the D-Region: A case Study Based Upon the 1966 Total Solar Eclipse," ASL-TR-0015, September 1978.

87. Jennings, S.G., and R.G. Pinnick, "Effects of Particulate Complex Refractive Index and Particle Size Distribution Variations on Atmospheric Extinction and Absorption for Visible Through Middle-Infrared Wavelengths," ASL-TR-0016, September 1978.

88. Watkins, Wendell R., Kenneth O. White, Lanny R. Bower, and Brian Z. Sojka, " Pressure Dependence of the Water Vapor Continuum Absorption in the 3.5- to 4.0-Micrometer Region," ASL-TR-0017, September 1978.

89. Miller, W.B., and B.F. Engebos, "Behavior of Four Sound Ranging Techniques in an Idealized Physical Enviroment," ASL-TR-0018, September 1978.

90. Gomez, Richard G., "Effectiveness Studies of the CBU-88/B Bomb, Cluster, Smoke Weapon" (U), CONFIDENTIAL ASL-TR-0019, September 1978.

91. Miller, August, Richard C. Shirkey, and Mary Ann Seagraves, "Calculation of Thermal Emission from Aerosols Using the Doubling Technique," ASL-TR-0020, November, 1978.

92. Lindberg, James D. et al., "Measured Effects of Battlefield Dust and Smoke on Visible, Infrared, and Millimeter Wavelengths Propagation: A Preliminary Report on Dusty Infrared Test-I (DIRT-I)," ASL-TR-0021, January 1979.

93. Kennedy, Bruce W., Arthur Kinghorn, and B.R. Hixon, "Engineering Flight Tests of Range Meteorological Sounding System Radiosonde," ASL-TR-0022, February 1979.

94. Rubio, Roberto, and Don Hoock, "Microwave Effective Earth Radius Factor Variability at Wiesbaden and Balboa," ASL-TR-0023, February 1979.

95. Low, Richard D.H., "A Theoretical Investigation of Cloud/Fog Optical Properties and Their Spectral Correlations," ASL-TR-0024, February 1979.

96. Pinnick, R.G., and H.J. Auvermann, "Response Characteristics of Knollenberg Light-Scattering Aerosol Counters," ASL-TR-0025, February 1979.
97. Heaps, Melvin G., Robert O. Olsen, and Warren W. Berning, "Solar Eclipse 1979, Atmospheric Sciences Laboratory Program Overview," ASL-TR-0026 February 1979.
98. Blanco, Abel J., "Long-Range Artillery Sound Ranging: 'PASS' GR-8 Sound Ranging Data," ASL-TR-0027, March 1979.
99. Kennedy, Bruce W., and Jose M. Serna, "Meteorological Rocket Network System Reliability," ASL-TR-0028, March 1979.
100. Swingle, Donald M., "Effects of Arrival Time Errors in Weighted Range Equation Solutions for Linear Base Sound Ranging," ASL-TR-0029, April 1979.
101. Umstead, Robert K., Ricardo Pena, and Frank V. Hansen, "KWIK: An Algorithm for Calculating Munition Expenditures for Smoke Screening/Obscuration in Tactical Situations," ASL-TR-0030, April 1979.
102. D'Arcy, Edward M., "Accuracy Validation of the Modified Nike Hercules Radar," ASL-TR-0031, May 1979.
103. Rodriguez, Ruben, "Evaluation of the Passive Remote Crosswind Sensor," ASL-TR-0032, May 1979.
104. Barber. T.L., and R. Rodgriquez, "Transit Time Lidar Measurement of Near-Surface Winds in the Atmosphere," ASL-TR-0033, May 1979.
105. Low, Richard D.H., Louis D. Duncan, and Y.Y. Roger R. Hsiao, "Microphysical and Optical Properties of California Coastal Fogs at Fort Ord," ASL-TR-0034, June 1979.
106. Rodriguez, Ruben, and William J. Vechione, "Evaluation of the Saturation Resistant Crosswind Sensor," ASL-TR-0035, July 1979.
107. Ohmstede, William D., "The Dynamics of Material Layers," ASL-TR-0036, July 1979.
108. Pinnick, R.G., S.G. Jennings, Petr Chylek, and H.J. Auvermann "Relationships between IR Extinction, Absorption, and Liquid Water Content of Fogs," ASL-TR-0037, August 1979.
109. Rodriguez, Ruben, and William J. Vechione, "Performance Evaluation of the Optical Crosswind Profiler," ASL-TR-0038, August 1979.
110. Miers, Bruce T., "Precipitation Estimation Using Satellite Data" ASL-TR-0039, September 1979.
111. Dickson, David H., and Charles M. Sonnenschein, "Helicopter Remote Wind Sensor System Description," ASL-TR-0040, September 1979.
112. Heaps, Melvin, G., and Joseph M. Heimerl, "Validation of the Dairchem Code, I: Quiet Midlatitude Conditions," ASL-TR-0041, September 1979.
113. Bonner, Robert S., and William J. Lentz, "The Visioceilometer: A Portable Cloud Height and Visibility Indicator," ASL-TR-0042, October 1979.
114. Cohn, Stephen L., "The Role of Atmospheric Sulfates in Battlefield Obscurations," ASL-TR-0043, October 1979.
115. Fawbush, E.J. et al, "Characterization of Atmospheric Conditions at the High Energy Laser System Test Facility (HELSTF), White Sands Missile Range, New Mexico, Part I, 24 March to 8 April 1977," ASL-TR-0044, November 1979
116. Barber, Ted L., "Short-Time Mass Variation in Natural Atmospheric Dust," ASL-TR-0045, November 1979
117. Low, Richard D.H., "Fog Evolution in the Visible and Infrared Spectral Regions and its Meaning in Optical Modeling," ASL-TR-0046, December 1979
118. Duncan, Louis D. et al, "The Electro-Optical Systems Atmospheric Effects Library, Volume I: Technical Documentation, ASL-TR-0047, December 1979.
119. Shirkey, R. C. et al, "Interim E-O SAEL, Volume II, Users Manual," ASL-TR-0048, December 1979.
120. Kobayashi, H.K., "Atmospheric Effects on Millimeter Radio Waves," ASL-TR-0049, January 1980.
121. Seagraves, Mary Ann and Duncan, Louis D., "An Analysis of Transmittances Measured Through Battlefield Dust Clouds," ASL-TR-0050, February, 1980.

122. Dickson, David H., and Jon E. Ottesen, "Helicopter Remote Wind Sensor Flight Test," ASL-TR-0051, February 1980.

123. Pinnick, R. G., and S. G. Jennings, "Relationships Between Radiative Properties and Mass Content of Phosphoric Acid, HC, Petroleum Oil, and Sulfuric Acid Military Smokes," ASL-TR-0052, April 1980.

124. Hinds, B. D., and J. B. Gillespie, "Optical Characterization of Atmospheric Particulates on San Nicolas Island, California," ASL-TR-0053, April 1980.

125. Miers, Bruce T.,"Precipitation Estimation for Military Hydrology,"ASL-TR-0054, April 1980.

126. Stenmark, Ernest R., "Objective Quality Control of Artillery Computer Meteorological Messages," ASL-TR-0055, April 1980.

127. Duncan, Louis D., and Richard D. H. Low, "Bimodal Size Distribution Models for Fogs at Meppen, Germany, " ASL-TR-0056, April 1980.

128. Olsen, Robert O., and Jagir S. Randhawa, "The Influence of Atmospheric Dynamics on Ozone and Temperature Structure," ASL-TR-0057, May 1980.

129. Kennedy, Bruce W., et al, "Dusty Infrared Test-II (DIRT-II) Program," ASL—TR-0058, May 1980.

130. Heaps, Melvin G., Roberts O. Olsen, Warren Berning, John Cross, and Arthur Gilcrease, "1979 Solar Eclipse,Part I - Atmospheric Sciences Laboratory Field Program Summary," ASL-TR-0059, May 1980.

131. Miller, Walter B.,"User's Guide for Passive Target Acquisition Program Two (PTAP-2)," ASL-TR-0060, June 1980.

132. Holt, E. H., editor, "Atmospheric Data Requirements for Battlefield Obscuration Applications, " ASL-TR-0061, June 1980.

133. Shirkey, Richard C., August Miller, George H. Goedecke, and Yugal Behl, "Single Scattering Code AGAUSX: Theory, Applications, Comparisons, and Listing," ASL—TR-0062, July 1980.

134. Sojka, Brain Z., and Kenneth O. White, "Evaluation of Specialized Photoacoustic Absorption Chambers for Near-millimeter Wave (NMMW) Propagation Measurements," ASL-TR-0063, August 1980.

135. Bruce, Charles W., Young Paul Yee, and S. G. Jennings, "In Situ Measurement of the Ratio of Aerosol Absorption to Extinction Coefficient," ASL-TR-0064, August 1980.

136. Yee, Young Paul, Charles W. Bruce, and Ralph J. Brewer, "Gaseous/Particulate Absorption Studies at WSMR using Laser Sourced Spectrophones," ASL-TR-0065, June 1980.

137. Lindberg, James D., Radon B. Loveland, Melvin Heaps, James B. Gillespie, and Andrew F.Lewis,"Battlefield Dust and Atmospheric Characterization Measurements During West German Summertime Conditions in Support of Grafenwohr Tests," ASL-TR-0066, September 1980.

138. Vechione, W. J., "Evaluation of the Environmental Instruments, Incorporated Series 200 Dual Component Wind Set, "ASL-TR-0067, September 1980.

139. Bruce, C. W., Y. P. Yee, B. D. Hinds, R. G. Pinnick, R. J. Brewer, and J. Minjares, "Initial Field Measurements of Atmospheric Absorption at 9μM to 11μM Wavelengths, " ASL-TR-0068, October 1980.

140. Heaps, M. G., R. O. Olsen, K. D. Baker, D. A. Burt, L. C. Howlett, L. L. Jensen, E. F. Pound, and G. D. Allred, "1979 Solar Eclipse: Part II Initial Results for Ionization Sources, Electron Density, and Minor Neutral Constituents," ASL-TR-0069, October 1980.

141. Low, Richard D. H., "One-Dimensional Cloud Microphysical Models for Central Europe and their Optical Properties," ASL-TR-0070, October 1980.

142. Duncan, Louis D., James D. Lindberg, and Radon B. Loveland, "An Empirical Model of the Vertical Structure of German Fogs," ASL-TR-0071, November 1980.

143. Duncan, Louis D., 1981, "EOSAEL 80, Volume I, Technical Documentation," ASL-TR-0072, January 1981.

144. Shirkey, R. C., and S. G. O'Brien "EOSAEL 80, Volume II, Users Manual," ASL-TR-0073, January 1981.

145. Bruce, C. W., "Characterization of Aerosol Nonlinear Effects on a High-Power CO_2 Laser Beam," ASL-TR-0074 , February 1981.

★U.S. GOVERNMENT PRINTING OFFICE: 1981-0-777-026/23